
Diffusion Models for Constrained Domains

Nic Fishman¹ Leo Klarner¹ Valentin De Bortoli² Emile Mathieu³ Michael Hutchinson¹

Abstract

Denoising diffusion models are a recent class of generative models which achieve state-of-the-art results in many domains such as unconditional image generation and text-to-speech tasks. They consist of a noising process destroying the data and a backward stage defined as the time-reversal of the noising diffusion. Building on their success, diffusion models have recently been extended to the Riemannian manifold setting. Yet, these Riemannian diffusion models require geodesics to be defined for all times. While this setting encompasses many important applications, it does not include manifolds defined via a set of inequality constraints, which are ubiquitous in many scientific domains such as robotics and protein design. In this work, we introduce two methods to bridge this gap. First, we design a noising process based on the *logarithmic barrier* metric induced by the inequality constraints. Second, we introduce a noising process based on the *reflected* Brownian motion. As existing diffusion model techniques cannot be applied in this setting, we derive new tools to define such models in our framework. We empirically demonstrate the applicability of our methods to a number of synthetic and real-world tasks, including the constrained conformational modelling of protein backbones and robotic arms.

1. Introduction

Diffusion models (Sohl-Dickstein et al., 2015; Song & Ermon, 2019; Song et al., 2021; Ho et al., 2020; Dhariwal & Nichol, 2021) have recently been introduced as a powerful new paradigm for generative modelling. They work as follows: noise is progressively added to data following a Stochastic Differential Equation (SDE)—the forward *noising* process—until it is approximately Gaussian. The generative model is given by an approximation of the asso-

ciated *time-reversed process* called the backward *denoising* process. This process is also an SDE whose drift depends on the gradient of the logarithm of the densities of the forward process, referred as the Stein score. This score is approximated by leveraging techniques from deep learning and score matching (Hyvärinen, 2005; Vincent, 2011).

Recently, this framework has been extended to a broad class of Riemannian manifolds, see De Bortoli et al. (2022); Huang et al. (2022), opening the door to many applications in the natural sciences (e.g. Trippe et al., 2022; Corso et al., 2022; Watson et al., 2022; Leach et al., 2022; Urain et al., 2022). In particular, this framework has been applied to Lie groups such as the group of rotations $SO(3)$ (Trippe et al., 2022; Corso et al., 2022) or the group of rigid body motions $SE(3)$ (Urain et al., 2022). However, both De Bortoli et al. (2022) and Huang et al. (2022) require that geodesics, i.e length minimising curves on the manifold, are defined for all times. As a consequence, this methodology cannot be applied to manifolds that are defined by a set of inequality constraints. Indeed, geodesics might then not be defined at all times, as illustrated on Figure 2. This rich class of constrained manifolds comprises a large variety of settings such as polytopes and convex sets of Euclidean spaces. These manifolds are ubiquitous in several scientific fields such as computational statistics and biology (Thiele et al., 2013; Morris, 2002; Lewis et al., 2012).

As sampling problems are also important on these manifolds (Kook et al., 2022; Heirendt et al., 2019), a flurry of Markov chain based methods have been developed to sample from unnormalised densities. Successful algorithms include the reflected Brownian motion (Williams, 1987; Petit, 1997; Shkolnikov & Karatzas, 2013), log-barrier methods (Kannan & Narayanan, 2009; Lee & Vempala, 2017; Noble et al., 2022; Kook et al., 2022; Gatmiry & Vempala, 2022; Lee & Vempala, 2018) and hit-and-run approaches in the case of polytopes (Smith, 1984; Lovász & Vempala, 2006).

In this work, we study the generative modelling counterparts of these algorithms through the lens of diffusion models. Among existing algorithms for statistical sampling on constrained manifolds, the reflected Brownian motion (Williams, 1987) and the geodesics Brownian motion (Lee & Vempala, 2017) are continuous stochastic processes, thus well suited for extending the continuous diffusion on manifolds framework developed by De Bortoli et al. (2022);

*Equal contribution ¹University of Oxford ²CNRS, ENS Ulm ³University of Cambridge. Correspondence to: Nic Fishman <nicolas.fishman@chch.ox.ac.uk>.

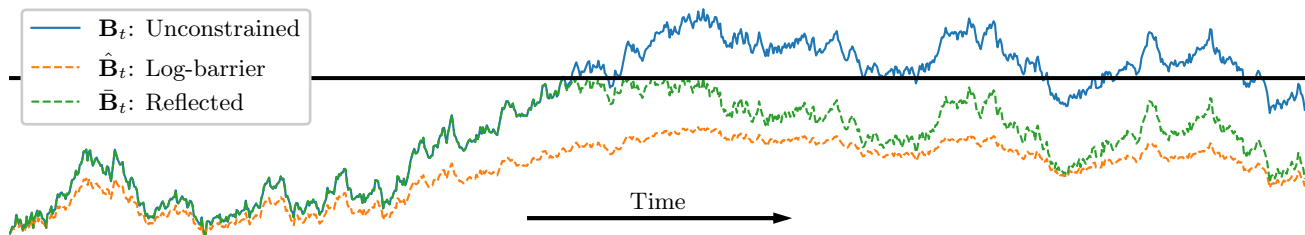


Figure 1: The behaviour of different types of noising processes considered in this work defined on the unit interval. \mathbf{B}_t : Euclidean (unconstrained) Brownian motion. $\hat{\mathbf{B}}_t$: Log barrier forward noising process. $\bar{\mathbf{B}}_t$: Reflected Brownian motion. All sampled with the same initial point and driving noise. Black line indicates the boundary.

Huang et al. (2022). This is what we achieve in this work. In particular, we introduce two principled diffusion models for generative modelling on constrained manifolds: a) one based on the geodesic Brownian motion, leveraging tools from the log-barrier methods, b) the other one based on the reflected Brownian motion. In both cases, we show how one can extend the ideas of time-reversal and score matching to these settings. We empirically demonstrate the scalability and flexibility of these methods on high-dimensional convex polytopes and symmetric positive definite matrices, with applications from robotics and protein design.

2. Background

Riemannian manifolds. A Riemannian manifold is a tuple $(\mathcal{M}, \mathbf{g})$ with \mathcal{M} a smooth manifold and \mathbf{g} a metric which defines an inner product on tangent spaces. The metric \mathbf{g} induces key quantities on the manifold, such as an exponential map $\exp_x : T_x\mathcal{M} \rightarrow \mathcal{M}$, the notion of following straight lines on manifolds, a gradient operator ∇^1 and a divergence operator div^2 . The metric induces the Laplace-Beltrami operator Δ and consequently a Brownian motion with density (w.r.t. the volume form³) whose density is given by the heat equation $\partial_t p_t = \Delta p_t$. We refer the reader to Appendix B for a brief introduction to differential geometry, to Lee (2013) for a thorough treatment and to Hsu (2002) for details on stochastic analysis on manifolds.

Constrained manifolds. In this work, we are concerned with *constrained* manifolds. More precisely, given a manifold $(\mathcal{N}, \mathbf{h})$, we consider a family of real functions $\{f_i : \mathcal{N} \rightarrow \mathbb{R}\}_{i \in \mathcal{I}}$ indexed by \mathcal{I} . We then define

$$\mathcal{M} = \{x \in \mathcal{N} : f_i(x) < 0, i \in \mathcal{I}\}. \quad (1)$$

¹The (Riemannian) gradient ∇ is defined s.t. for any smooth $f \in C^\infty(\mathcal{M})$, $x \in \mathcal{M}$, $v \in T_x\mathcal{M}$, $\mathbf{g}(x)(\nabla f(x), v) = \text{d}f(x)(v)$.

²The Riemannian divergence acts vector fields and can be defined using the volume form of \mathcal{M} .

³We assume that \mathcal{M} is orientable and therefore that a volume form exists.

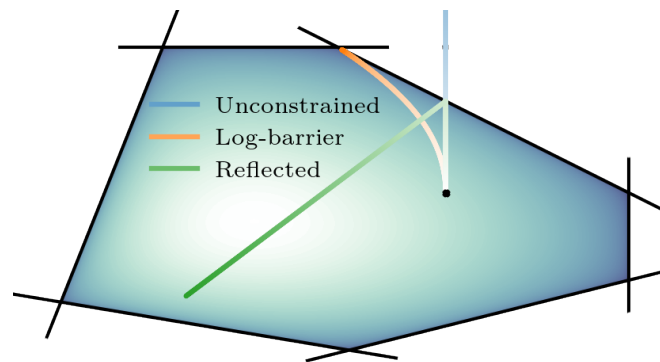


Figure 2: A convex polytope defined by six constraints $\{f_i\}_{i \in \mathcal{I}}$, along with the log barrier potential, and ‘straight trajectories’ under the log-barrier metric and under the Euclidean metric with and without reflection at the boundary.

In this scenario, $\{f_i\}_{i \in \mathcal{I}}$ is interpreted as a set of constraints on \mathcal{N} . This setting encompasses a large class of (topological) manifolds. For instance, using the Hahn-Banach theorem (Brezis & Brézis, 2011, Chapter 1, Theorem 1.7), it can be shown that every closed convex set can be described using (1)⁴. Similarly, with affine constraints $f_i(x) = \langle a_i, x \rangle - b_i$, $x \in \mathbb{R}^d$, we get a polytope as illustrated in Figure 2.

Additionally, since sampling from a distribution defined on a manifold described by (1) can be understood as sampling from a distribution whose supports is defined by *constraints*, this setting naturally appears in many areas of science (Han & Rudolph, 2006). While the two methods we introduce in Section 3 can be applied to the general framework (1), in our applications, we focus on two specific settings: (a) polytopes— $\mathcal{N} = \mathbb{R}^d$, (b) symmetric positive definite matrices (SPD) under trace conditions— $\mathcal{N} = \mathcal{S}^{++}(d)$.

Continuous diffusion models. We briefly recall the framework for constructing continuous diffusion processes introduced by Song et al. (2021) in the context of generative

⁴Replacing $<$ by \leq .

modelling over \mathbb{R}^d . First, we consider a forward *noising process* $(\mathbf{X}_t)_{t \in [0, T]}$ which progressively noise a data distribution p_0 into a Gaussian $N(0, \text{Id})$. In particular we consider an Ornstein–Uhlenbeck (OU) process which is defined by the following stochastic differential equation (SDE)

$$d\mathbf{X}_t = -\frac{1}{2}\mathbf{X}_t dt + d\mathbf{B}_t, \quad \mathbf{X}_0 \sim p_0.$$

Under mild conditions on p_0 , the time-reversed process $(\overleftarrow{\mathbf{X}}_t)_{t \in [0, T]} = (\mathbf{X}_{T-t})_{t \in [0, T]}$ also satisfies an SDE (Cattiaux et al., 2021; Haussmann & Pardoux, 1986) given by

$$d\overleftarrow{\mathbf{X}}_t = \left\{ \frac{1}{2}\overleftarrow{\mathbf{X}}_t + \nabla \log p_{T-t}(\overleftarrow{\mathbf{X}}_t) \right\} dt + d\mathbf{B}_t, \quad \overleftarrow{\mathbf{X}}_0 \sim p_T, \quad (2)$$

where p_t denotes the density of \mathbf{X}_t . The quantity $\nabla \log p_t$ is referred as the Stein score and is unavailable in practice. It can be approximated with a score network $s_\theta(t, \cdot)$ trained by minimising an implicit score matching (ism) loss

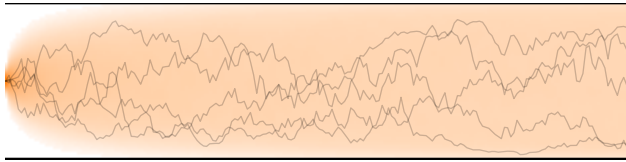
$$\mathcal{L}(\theta) = \mathbb{E}[\lambda_t \left\{ \frac{1}{2} \|s_\theta(t, \mathbf{X}_t)\|^2 + \text{div}(s_\theta)(t, \mathbf{X}_t) \right\}], \quad (3)$$

where $\lambda_t > 0$ is a weighting function, and the expectation is taken over $t \sim \mathcal{U}([0, T])$ and $(\mathbf{X}_0, \mathbf{X}_t)$. For an arbitrarily flexible score network, the global minimiser $\theta^* = \text{argmin}_\theta \mathcal{L}(\theta)$ satisfies $s_{\theta^*}(t, \cdot) = \nabla \log p_t$.

3. Inequality constrained diffusion models

We are now ready to introduce our methodology to deal with manifolds defined via inequality *constraints* (1). We first propose in Section 3.1, a Riemannian diffusion model endowed with a metric induced by a log-barrier potential. In Section 3.2, we introduce a *reflected* diffusion model. While both models extend classical diffusion models to the inequality constrained settings, they exhibit very different behaviour. We discuss their practical differences in Section 5.1.

3.1. Log-barrier diffusion models



$$d\mathbf{X}_t = \frac{1}{2} \text{div}(\mathbf{g}^{-1})(\mathbf{X}_t) dt + \mathbf{g}^{-1/2}(\mathbf{X}_t) d\mathbf{B}_t$$

Figure 3: Convergence of the Barrier Langevin dynamics on the unit interval to the uniform distribution.

Barrier Langevin Dynamics. Barrier methods work by constructing a smooth potential $\phi : \mathcal{M} \rightarrow \mathbb{R}$ such that it blows up on the boundary of a desired set, see Nesterov et al. (2018). Such potentials are at the basis of interior methods in

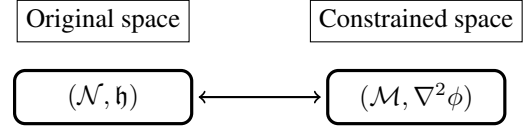


Figure 4: Illustrative diagram of the barrier method and the change of metric.

optimisation (Boyd et al., 2004). Among these functions, the *logarithmic barrier* is the most popular among practitioners (Lee & Vempala, 2017). For a convex polytope \mathcal{M} defined by the constraints $Ax < b$, the logarithmic barrier is given for any $x \in \mathcal{M}$ by

$$\phi(x) = -\sum_{i=1}^m \log(\langle A_i, x \rangle - b_i). \quad (4)$$

Assuming that $\|A_i\| = 1$, we have that for any $x \in \mathcal{M}$, $\phi(x) = -\sum_{i=1}^m \log(d(x, \partial\mathcal{M}_i))$, where $\partial\mathcal{M}_i = \{x \in \mathbb{R}^d : \langle A_i, x \rangle = b\}$. The core idea of barrier methods is to ‘warp the geometry’ of the constrained space, so that sampling on this warped space bypasses the need to explicitly deal with the boundary, whilst ensuring that the returned samples are distributed according to the target distribution on the original space (and w.r.t. the original metric)—see Figure 4. Assuming ϕ to be strictly convex and smooth—which is for example verified for (4)—its Hessian $\nabla^2 \phi$ is positive definite thus it defines a valid Riemannian metric. The formal approach to ‘transforming the geometry’ of the convex space with boundary, is to endow that space with the Riemannian metric $\mathbf{g} = \nabla^2 \phi$, thus referred as Hessian manifolds. For (4), we have that $\mathbf{g}(x) = A^\top S^{-2}(x)A$ with $S(x) = \text{diag}(b_i - \langle A_i, x \rangle)_i$.

Let’s consider the following Langevin dynamics as the forward process (Lee & Vempala, 2017)

$$d\mathbf{X}_t = \frac{1}{2} \text{div}(\mathbf{g}^{-1})(\mathbf{X}_t) dt + \mathbf{g}(\mathbf{X}_t)^{-\frac{1}{2}} d\mathbf{B}_t, \quad (5)$$

with $\text{div}(F)(x) \triangleq (\text{div}(F_1)(x), \dots, \text{div}(F_d)(x))^\top$, for any smooth $F : \mathbb{R}^d \rightarrow \mathbb{R}^d$. Denoting p_t the density of \mathbf{X}_t , we have that $\partial_t p_t = \text{Tr}(\mathbf{g}^{-1} \nabla^2 p_t)$, see Appendix C for more details on this process. Hence, assuming that \mathcal{M} is compact, the uniform distribution on \mathcal{M} , is the invariant measure and we have that the distribution of $(\mathbf{X}_t)_{t \geq 0}$ converges exponentially fast towards the uniform, see Lee & Vempala (2017, Theorem 23).

Time-reversal. Assuming that \mathbf{g}^{-1} and its derivative are bounded on \mathcal{M} , the time-reversal of (5) is given by Cattiaux et al. (2021), in particular we have

$$\begin{aligned} d\overleftarrow{\mathbf{X}}_t &= \left[-\frac{1}{2} \text{div}(\mathbf{g}^{-1}) + \text{div}(\mathbf{g}^{-1}) \right. \\ &\quad \left. + \mathbf{g}^{-1} \nabla \log p_{T-t} \right] (\overleftarrow{\mathbf{X}}_t) dt + \mathbf{g}(\overleftarrow{\mathbf{X}}_t)^{-\frac{1}{2}} d\mathbf{B}_t, \quad (6) \\ &= \left[\frac{1}{2} \text{div}(\mathbf{g}^{-1}) + \mathbf{g}^{-1} \nabla \log p_{T-t} \right] (\overleftarrow{\mathbf{X}}_t) dt + \mathbf{g}(\overleftarrow{\mathbf{X}}_t)^{-\frac{1}{2}} d\mathbf{B}_t. \end{aligned}$$

$\overleftarrow{\mathbf{X}}_0$ is initialised with the uniform distribution on \mathcal{M} (which is close to the one of \mathbf{X}_T for large T). Practically, one can obtain samples from the uniform reference distribution (w.r.t the original metric) using any MCMC converging to this stationary distribution. In this work, we focus on the *hit-and-run* algorithm (Claude J. P. Bélisle et al., 1993), which we found to be converging very fast to the uniform in our polytope settings. The estimation of the score term $\nabla \log p_t$ is done by minimising the ism loss function (3). We refer to Section 3.3 for details on the training and parameterisation.

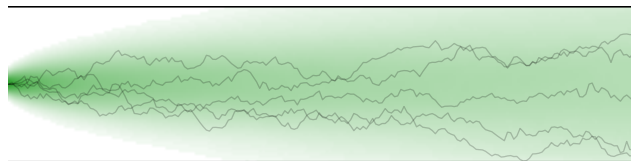
Sampling. Sampling from the forward (5) and backward (6) processes, once the score is learnt, requires a discretisation scheme. We use Geodesic Random Walks (GRW) (Jørgensen, 1975) for this purpose, see Algorithm 1. This discretisation is a generalisation of the Euler-Maruyama discretisation of SDE in Euclidean spaces, where the $+$ operator is replaced by the exponential mapping on the manifold, computing the geodesics. However, contrary to (De

Algorithm 1 *Geodesic Random Walk.* Discretisation of the SDE $d\mathbf{X}_t = b(t, \mathbf{X}_t)dt + d\mathbf{B}_t$.

Require: T, N, X_0^γ, b
 $\gamma = T/N$
for $k \in \{0, \dots, N-1\}$ **do**
 $Z_{k+1} \sim \mathcal{N}(0, \text{Id})$
 $W_{k+1} = \gamma b(k\gamma, X_k) + \sqrt{\gamma} Z_{k+1}$
 $X_{k+1}^\gamma = \exp_{X_k}[W_{k+1}] \approx \text{proj}_{\mathcal{M}}(X_k + W_{k+1})$
return $\{X_k\}_{k=0}^N$

Bortoli et al., 2022), we do not have access explicitly to the exponential mapping. Instead, we rely on an approximation, using a *retraction*, see Ablin & Peyré (2022) for a definition and alternative schemes. We also emphasise that the log-likelihood of the model can be evaluated using the equivalent ODE to (6), see Appendix E for more details.

3.2. Reflected diffusion models



$$d\bar{\mathbf{B}}t = d\mathbf{B}t - d\mathbf{k}_t$$

Figure 5: Convergence of the reflected Brownian motion on the unit interval to the uniform distribution.

Another approach to deal with the geometry of \mathcal{M} is to leave the metric g of \mathcal{M} untouched, but instead to consider an *unconstrained* forward dynamics on \mathcal{N} , and then restraining it to \mathcal{M} by considering a *reflected* version of the process.

To simplify the presentation we focus on the case $\mathcal{N} = \mathbb{R}^d$ and $\partial\mathcal{M}$ to be smooth⁵. We also assume that \mathcal{M} is compact and convex. In the next paragraph, we formally introduce the *reflected Brownian motion*.

Skorokhod problem. We say that $(\bar{\mathbf{B}}_t, \mathbf{k}_t)_{t \geq 0}$ is a solution to the *Skorokhod problem* (Skorokhod, 1961) if $(\mathbf{k}_t)_{t \geq 0}$ is a bounded variation process and $(\bar{\mathbf{B}}_t)_{t \geq 0}$ a continuous adapted process such that for any $t \geq 0$,

$$\bar{\mathbf{B}}_t = \bar{\mathbf{B}}_0 + \mathbf{B}_t - \mathbf{k}_t \in \mathcal{M}, \quad (7)$$

and $|\mathbf{k}|_t = \int_0^t \mathbf{1}_{\bar{\mathbf{B}}_s \in \partial\mathcal{M}} d|\mathbf{k}|_s$, $\mathbf{k}_t = \int_0^t \mathbf{n}(\bar{\mathbf{B}}_s) d|\mathbf{k}|_s$, where $(|\mathbf{k}|_t)_{t \geq 0}$ is the total variation of $(\mathbf{k}_t)_{t \geq 0}$. The condition $|\mathbf{k}|_t = \int_0^t \mathbf{1}_{\bar{\mathbf{B}}_s \in \partial\mathcal{M}} d|\mathbf{k}|_s$ can be interpreted as \mathbf{k}_t being constant when $(\bar{\mathbf{B}}_t)_{t \geq 0}$ does not hit the boundary. When $(\bar{\mathbf{B}}_t)_{t \geq 0}$ hits the boundary, the condition $\mathbf{k}_t = \int_0^t \mathbf{n}(\bar{\mathbf{B}}_s) d|\mathbf{k}|_s$, tells us that $-\mathbf{k}_t$ “compensates” for $\bar{\mathbf{B}}_t$ by pushing the process back into \mathcal{M} along the inward normal $-\mathbf{n}$. As a result $(\bar{\mathbf{B}}_t)_{t \geq 0}$ can be understood as the continuous-time counterpart to the reflected Gaussian random walk. The process $(\mathbf{k}_t)_{t \geq 0}$ can be related to the notion of *local time* (Revuz & Yor, 2013) and quantify the amount of time $(\bar{\mathbf{B}}_t)_{t \geq 0}$ spends at the boundary $\partial\mathcal{M}$. Lions & Sznitman (1984, Theorem 2.1) ensure the existence and uniqueness of a solution to the Skorokhod problem. One key observation is that the event $\{\bar{\mathbf{B}}_t \in \partial\mathcal{M}\}$ has probability zero (Harrison & Williams, 1987, Section 7, Lemma 7). As in the *unconstrained* setting, one can describe the dynamics of the density of $\bar{\mathbf{B}}_t$.

Proposition 3.1 (Burdzy et al. (2004)). *For any $t > 0$, the distribution of $\bar{\mathbf{B}}_t$ admits a density w.r.t. the Lebesgue measure denoted p_t . In addition, we have for any $x \in \text{int}(\mathcal{M})$ and $x_0 \in \partial\mathcal{M}$*

$$\partial_t p_t(x) = \frac{1}{2} \Delta p_t(x), \quad \partial_{\mathbf{n}} p_t(x_0) = 0, \quad (8)$$

where we recall that \mathbf{n} is the outward normal.

Note that contrary to the unconstrained setting, the heat equation has *Neumann* boundary conditions. Similarly to the compact Riemannian setting (Saloff-Coste, 1994) it can be shown that the reflected Brownian motion converges to the uniform distribution on \mathcal{M} exponentially fast (Loper, 2020), see Figure 5. Hence, $(\bar{\mathbf{B}}_t)_{t \geq 0}$ is a candidate for a forward noising process in the context of diffusion models.

Time-reversal. In order to extend the diffusion model approach to the reflected setting, we need to derive a *time-reversal* for $(\bar{\mathbf{B}}_t)_{t \in [0, T]}$. Namely, we need to characterise the evolution of $(\overleftarrow{\mathbf{X}}_t)_{t \in [0, T]} = (\bar{\mathbf{B}}_{T-t})_{t \in [0, T]}$. It can be shown that the time-reversal of $(\bar{\mathbf{B}}_t)_{t \in [0, T]}$ is also the solution to a Skorokhod problem.

⁵We refer to Appendix G for a definition of smooth boundary.

Theorem 3.2. *There exist $(\overleftarrow{\mathbf{k}}_t)_{t \geq 0}$ a bounded variation process and a Brownian motion $(\mathbf{B}_t)_{t \geq 0}$ such that*

$$\overleftarrow{\mathbf{X}}_t = \overleftarrow{\mathbf{X}}_0 + \mathbf{B}_t + \int_0^t \nabla \log p_{T-s}(\overleftarrow{\mathbf{X}}_s) ds - \overleftarrow{\mathbf{k}}_t.$$

In addition, for any $t \in [0, T]$ we have

$$\overleftarrow{\mathbf{k}}|_t = \int_0^t \mathbf{1}_{\overleftarrow{\mathbf{X}}_s \in \partial \mathcal{M}} d\overleftarrow{\mathbf{k}}|_s, \quad \overleftarrow{\mathbf{k}}_t = \int_0^t \mathbf{n}(\overleftarrow{\mathbf{X}}_s) d\overleftarrow{\mathbf{k}}|_s.$$

The proof, see Appendix G, follows Petit (1997) which provides a time-reversal in the case where \mathcal{M} is the positive orthant. It is based on an extension of Haussmann & Pardoux (1986) to the reflected setting, with a careful handling of the boundary conditions. In particular, contrary to Petit (1997), we do not rely on an explicit expression of p_t but instead use the intrinsic properties of $(\mathbf{k}_t)_{t \geq 0}$. Informally, Theorem 3.2 means that the process $(\overleftarrow{\mathbf{X}}_t)_{t \in [0, T]}$ satisfies

$$d\overleftarrow{\mathbf{X}}_t = \nabla \log p_{T-t}(\overleftarrow{\mathbf{X}}_t) dt + d\mathbf{B}_t - d\overleftarrow{\mathbf{k}}_t, \quad (9)$$

which echoes the usual time-reversal formula (2). In practice, in order to sample from $(\overleftarrow{\mathbf{X}}_t)_{t \in [0, T]}$, one need to consider the *reflected* version of the *unconstrained* dynamics $d\overleftarrow{\mathbf{X}}_t = \nabla \log p_{T-t}(\overleftarrow{\mathbf{X}}_t) dt + d\mathbf{B}_t$. The next proposition ensures that the ism loss is still valid in this reflected setting.

Proposition 3.3. *Let $s \in C^\infty([0, T] \times \mathbb{R}^d, \mathbb{R}^d)$ such that for any $x \in \partial \mathcal{M}$ and $t \geq 0$, $s_t(x) = 0$. Then, there exists $C > 0$ such that*

$$\mathbb{E}[\|\nabla \log p_t - s_t\|^2] = \mathbb{E}[\|s_t\|^2] + 2 \operatorname{div}(s_t) + C,$$

where \mathbb{E} is taken over $\mathbf{X}_t \sim p_t$ and $t \sim \mathcal{U}([0, T])$.

The estimation of the score term $\nabla \log p_t$ is also done by minimising the ism loss function (3), see Section 3.3 for details on the training and parameterisation of the score.

Sampling. In practice, we approximately sample the reflected dynamics by considering the Markov chain given by Algorithm 3. We refer to Pacchiarotti et al. (1998); Bossy et al. (2004) for weak convergence results on this numerical scheme in the Euclidean setting.

3.3. Score network parametrisation and training

The score term $\nabla \log p_{T-t}$ appearing in both time-reversal processes (6) and (9) is intractable. It is thus approximated with a *score network* $s_\theta(t, \cdot) \approx \nabla \log p_t$. We use a multi-layer perceptron architecture with sin activation functions, see Appendix J for more details on the experimental setup. Due to boundary condition (8), the normal component of the score is zero at the boundary in the reflected case. A similar result holds in the log-barrier setting. We include this in our score parameterisation by scaling the output of the neural

Algorithm 2 Reflected step algorithm. The algorithm operates by repeatedly taking geodesic steps until one of the constraint is violated, or the step is fully taken. Upon hitting the boundary we parallel transport the tangent vector to the boundary and then reflect it against the boundary. We then start a new geodesic from this point in the new direction. The $\operatorname{arg\,intersect}_t$ function computes the distance one must travel along a geodesic in direction \mathbf{s} til constraint f_i is intersected. For a discussion of paralleltransport, \exp_g and reflect please see Appendix B

Require: $x \in \mathcal{M}, \mathbf{v} \in \mathbb{T}_x \mathcal{M}, \{f_i\}_{i \in \mathcal{I}}$
 $\ell \leftarrow \|\mathbf{v}\|_g$
 $\mathbf{s} \leftarrow \mathbf{v} / \|\mathbf{v}\|_g$
while $\ell \geq 0$ **do**
 $d_i = \operatorname{arg\,intersect}_t[\exp_g(x, t\mathbf{s}), f_i]$
 $i \leftarrow \operatorname{argmin}_i d_i \text{ s.t. } d_i > 0$
 $\alpha \leftarrow \min(d_i, \ell)$
 $x' \leftarrow \exp_g(x, \alpha \mathbf{s})$
 $\mathbf{s} \leftarrow \operatorname{paralleltransport}_g(x, \mathbf{s}, x')$
 $\mathbf{s} \leftarrow \operatorname{reflect}(\mathbf{s}, f_i)$
 $\ell \leftarrow \ell - \alpha$
 $x \leftarrow x'$
return x

Algorithm 3 Reflected Random Walk. Discretisation of the SDE $d\mathbf{X}_t = b(t, \mathbf{X}_t) dt + d\mathbf{B}_t - d\mathbf{k}_t$.

Require: $T, N, X_0^\gamma, \{f_i\}_{i \in \mathcal{I}}$
 $\gamma = T/N$
for $k \in \{0, \dots, N-1\}$ **do**
 $Z_{k+1} \sim \mathcal{N}(0, \operatorname{Id})$
 $X_{k+1}^\gamma = \operatorname{ReflectedStep}[X_k^\gamma, \sqrt{\gamma} Z_{k+1}, \{f_i\}_{i \in \mathcal{I}}]$
return $\{X_k^\gamma\}_{k=0}^N$

network as $s_\theta(t, x) = \operatorname{ReLU}(d(x, \partial \mathcal{M}) - \delta) \cdot \operatorname{NN}_\theta(t, x)$ with $\delta > 0$ a threshold, see Appendix J for an illustration. The weighting function in (3) is set to $\lambda_t = (t + 1)$.

The forward processes (5) and (7) for the barrier and reflected methods cannot be sampled in closed form, so at training time samples from the conditional marginals $p(\mathbf{X}_t | \mathbf{X}_0)$ are obtained by discretising these processes. As to take the most of this computational overhead, we use several samples from the discretised forward trajectory $(\mathbf{X}_{t_1}, \dots, \mathbf{X}_{t_k} | \mathbf{X}_0)$ instead of only using the last sample.

4. Related Work

Sampling on constrained manifolds. Sampling from a distribution on a space defined by a set of constraints is an important ingredient in several computational tasks, such as computing the volume of a polytope (Lee & Vempala, 2017). Incorporating such constraints inside MCMC algo-

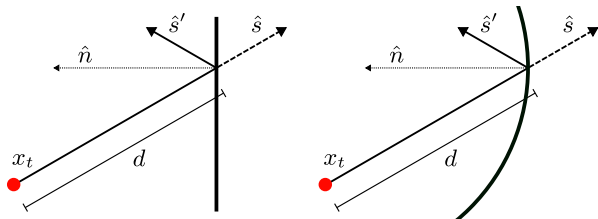


Figure 6: *Left*: Reflection against a linear boundary. For a step s with magnitude $|s|$ and direction \hat{s} the distance to the boundary described by the normal \hat{n} and offset b is $d = \frac{\langle \hat{s}, x_t \rangle - b}{\langle \hat{s}, \hat{n} \rangle}$. The reflected direction is given by $\hat{s}' = \hat{s} - 2\langle \hat{s}, \hat{n} \rangle \hat{n}$. *Right*: Reflection against a spherical boundary. For a sphere of radius r , the distance to the boundary from x_t in direction s is given by $d = \frac{1}{2}(\langle \hat{s}, x_t \rangle^2 + 4(r^2 - \|x_t\|^2))^{1/2} - \frac{1}{2}\langle \hat{s}, x_t \rangle$. The normal at the intersection can be computed as the unit vector in the direction $-2(d\hat{s} + x_t)$, and then \hat{s}' as above.

gorithms while preserving fast convergence properties is an active field of research (Kook et al., 2022; Lee & Vempala, 2017; Noble et al., 2022). In this work, we are interested in sampling from the uniform distribution defined on the constrained set in order to define a proper *forward process* for our diffusion model. Log-barrier methods such as the Dikin walk or Riemannian Hamiltonian Monte Carlo (Kannan & Narayanan, 2009; Lee & Vempala, 2017; Noble et al., 2022) change the geometry of the underlying space and define stochastic processes which never violate the constraints, see (Kannan & Narayanan, 2009; Noble et al., 2022) for instance. If we keep the Euclidean metric, then a classical random walk discretising the Brownian motion will almost surely violate the constraints. The manifold is said to be geodesically not complete. To counter this effect, it has been proposed to *reflect* the Brownian motion (Williams, 1987; Petit, 1997; Shkolnikov & Karatzas, 2013). Finally, we also highlight hit-and-run approaches (Smith, 1984; Lovász & Vempala, 2006) which generalise Gibbs’ algorithm and enjoy fast convergence properties provided that one knows how to sample from the one-dimensional marginals.

Diffusion models on manifolds. De Bortoli et al. (2022) extended the work of Song et al. (2021) to Riemannian manifolds by defining forward and backward stochastic processes in this setting. Concurrently, a similar framework was introduced by Huang et al. (2022) extending the maximum likelihood approach of Huang et al. (2021). Existing applications of denoising diffusion models on Riemannian manifolds have been focused on well-known manifolds for which one can find metrics so that the framework of De Bortoli et al. (2022) applies. In particular, on compact Lie groups, geodesics and Brownian motions can be defined in a canonical manner. Leach et al. (2022) define diffusion models on $\text{SO}(3)$ for rotational alignment, while Jing et al.

(2022) consider the product of tori for molecular conformer generation. Corso et al. (2022) use diffusion models on $\mathbb{R}^3 \times \text{SO}(3) \times \text{SO}(2)$ for protein docking applications. Finally, Urain et al. (2022) introduce a methodology for $\text{SE}(3)$ diffusion models with applications to robotics.

5. Experimental results

To illustrate the modelling ability of the constrained diffusion models introduced in Section 3, we first construct a series of increasingly difficult synthetic tasks on convex polytopes such as the hypercube and simplex in Section 5.1. We then demonstrate their practical applicability for two real-world problems from robotics and molecular biology. In particular in Section 5.2, we show that these models are able to model distributions on the space of $d \times d$ symmetric positive definite (SPD) matrices S_{++}^d under trace constraints, a setting that is essential to describing and controlling the motions and exerted forces of robotic platforms (Yoshikawa, 1985). Our dataset is taken from (Jaquier et al., 2021), see Appendix I for details. In Section 5.3, we map the problem of modelling the conformational ensembles of proteins under positional constraints on their endpoints, to the product manifold of a convex polytope and a torus (Han & Rudolph, 2006). We refer the reader to Appendix J for more details on the experimental setup. Additionally, the codebase will be made public upon publication.

5.1. Convex polytopes and methods comparison

Synthetic data. First, we aim to assess the ability of our proposed methods to scale with the space dimensionality. We focus on polytopes, and construct synthetic datasets from bimodal distributions. We recall that a polytope is an open set in \mathbb{R}^d with affine constraints, i.e. such that $Ax < b$, $A \in \mathbb{R}^{p \times d}$ and $b \in \mathbb{R}^p$. In particular we investigate two specific instances of polytopes: hypercubes and simplices. In Appendix J.1 we also present results on the Birkhoff polytope. We measure the performance of trained models via the Maximum Mean Discrepancy (MMD) (Gretton et al., 2012), which is a kernel based metric between distributions.

Comparison. On Figure 7, we qualitatively observe that both methods recover the data distribution on the two-dimensional hypercube and simplex, although the reflected method seem to have a better fit. In Table 1, we report the MMD between the data distribution and the learnt diffusion models. We similarly observe that the reflected method consistently gives better results than the log-barrier one. One key drawback of the log-barrier method is the slow convergence of the forward, which can already be seen in Figure 3. It should also be highlighted that in order to implement the log-barrier method, one needs in general to invert a $d \times d$ matrix, which can be implemented using $O(d^3)$ operations.

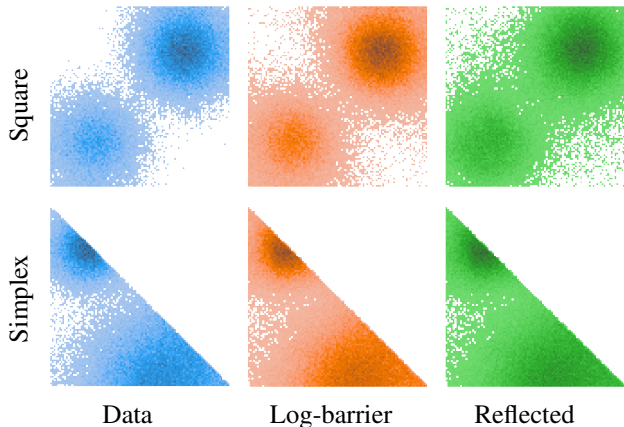


Figure 7: Histograms of samples from the data distribution and from trained constrained diffusion models.

Table 1: MMD metrics between synthetic data of varying dimension and samples from trained constrained diffusion models. Bold indicates best results.

Space	Dimension	Log-barrier	Reflected
Δ^d	2	0.05	0.02
	3	0.10	0.09
	10	0.17	0.07
$[-1, 1]^d$	2	0.03	0.03
	3	0.05	0.06
	10	0.26	0.06

This prevents the use of the log-barrier method for very high dimensional applications. On the other hand, the likelihood evaluation tools from Riemannian diffusion models (De Bortoli et al., 2022, Appendix D) can readily be adapted to the log-barrier method, while no straightforward equivalent exists for the reflected method (see Appendix E).

5.2. Learning constrained SPD matrices for robotic arms modelling

Accurately determining and controlling the movement and exerted forces of a robotic platform is a fundamental problem in many real-world robotics applications (Yoshikawa, 1985). A kinetostatic descriptor that is commonly used to quantify the ability of a robotic arm to move and apply forces along certain dimensions is the so-called manipulability ellipsoid $E \in \mathbb{R}^d$ (Yoshikawa, 1985) which is naturally described as a symmetric positive definite (SPD) matrix $M \in \mathbb{R}^{d \times d}$ (Jaquier et al., 2021). The manifold of such $d \times d$ SPD matrices, denoted as S_{++}^d , is defined as the set of matrices $\{x^T M x \geq 0, x \in \mathbb{R}^d : M \in \mathbb{R}^{d \times d}\}$.

In many practical settings, it may be desirable to constrain the volume of E to retain flexibility or limit the magnitude

of an exerted force, which can be expressed as an upper bound on the trace of M , i.e. as the inequality constraint $\sum_{i=1}^d M_{ii} < C$ with $C > 0$. Constraining the rest of the entries of the matrix to ensure it is SPD is non-trivial.

Alternatively, we can parameterise the SPD matrices via their Cholesky decomposition. Each SPD matrix has a unique decomposition of the form $M = LL^T$, where L is a lower triangular matrix with strictly positive diagonal (Golub & Van Loan, 2013, p.143). Constraining the entries of this matrix simply requires ensuring the diagonal is positive. The trace of the SPD matrix is given by $\text{Tr}(M) = \text{Tr}(LL^T) = \sum_{ij} L_{ij}^2$, and results in the constraint on the entries of L to live in a ball of radius C .

We additionally model the two-dimensional position of the arm. In summary, the space over which we parameterise the diffusion models is defined as $\{L \in \mathbb{R}^{d(d+1)/2} : L_{i,i} > 0, \sum_{i,j} L_{i,j}^2 < C\} \times \mathbb{R}^2$. Under the Euclidean metric we can apply both our log-barrier and reflected approaches. The positive diagonal (linear) constraint is handled similarly as in the polytope setting. The reflection on the ball boundary is defined and illustrated on Figure 6. In Figure 9, we plot the joint distribution over the SPD matrices (represented as ellipsoids) and their positions. We qualitatively observe that the reflected method is able to fit the joint data distribution. Quantitatively, the reflected method achieves an MMD of 0.161 as opposed to 0.247 for the log-barrier one.

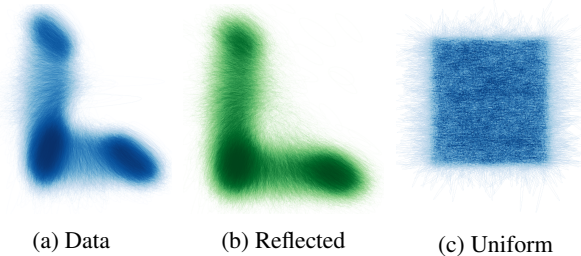


Figure 9: Samples of joint distributions over SPD matrices (illustrated as ellipsoids) and their location, see Appendix J for additional results and pair plots.

5.3. Modelling protein backbones with anchored endpoints

Modelling the conformational ensembles of proteins is an important task in the field of molecular biology, particularly in the context of bioengineering and drug design. In many data-scarce settings, it may be unnecessary to model the structure of an entire protein, as researchers are primarily interested in specific functional sites. However, only generating conformations for a subset of a protein requires positional constraints on its endpoints to ensure that it can still be accommodated by the remaining scaffold. More generally, this is the problem of how to model a chain with

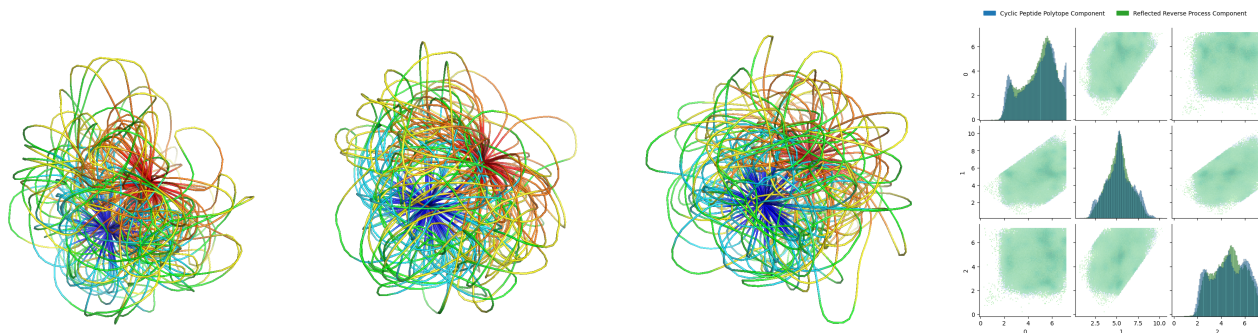


Figure 8: (a-c) 100 polypeptides samples—modelled as chain of C_α atoms—from the training dataset, a trained reflected model and from the uniform distribution over the polytope and torus product $\mathbb{P}^3 \times \mathbb{T}^4$ ((a) groundtruth, (b) output of our method, (c) sample from the uniform distribution). (d) Pairwise comparison of the polytope components of the target distribution over cyclic peptides and samples from the reflected method. Additional results and similar plots for the log barrier method are postponed to Appendix J.

fixed end points.

We follow the framework outlined in Han & Rudolph (2006) for parameterising an end-points-constrained chain with d links as the product of a convex polytope \mathbb{P} and torus \mathbb{T} : $\mathbb{P}^{(d-2)} \times \mathbb{T}^{(d-1)}$. The essential idea in this parameterisation is to fix one end point as an “anchor” and model the chain as the series of triangles formed by the anchor and each pair of sequential joints in the chain. A point in the polytope corresponds to the lengths of the diagonals of these triangles, and the point in the torus to the angles between each subsequent triangle. See Appendix H.1 for more details.

Using this framework, we model the (smoothed) energetic landscape of the conformations of cyclic peptides of length 6, i.e. circular polypeptide chains with coinciding end-points, as a distribution over $\mathbb{P}^3 \times \mathbb{T}^4$. We then draw samples on this product manifold from a Boltzmann distribution parametrised by molecular dynamics potentials (using OPENMM (Eastman et al., 2017) and AMBER (Hornak et al., 2006)), which we subsequently divide into training and evaluation datasets, see Appendix H.2. The space on which we effectively parameterise the reflected diffusion model is thus the product space $\mathbb{P}^3 \times \mathbb{T}^4$, leveraging the methodology introduced in Section 3.2 for the polytope \mathbb{P}^3 component and in De Bortoli et al. (2022) for the torus \mathbb{T}^4 part.

Figure 8 shows samples from the data distribution, along with generated samples from our learnt reflected diffusion model. From (d) we can see that on the polytope component we successfully learn the modes of the distribution. This translates into the visualisation of the loops in (a-c) where we can see a pronounced gap in the conformational space occupied by samples from the data distribution and the reflected method that is not apparent for uniform samples.

6. Discussion

Learning complex distributions supported on constrained spaces is of importance in several fields of the natural sciences, such as computational biology, see Han & Rudolph (2006). In this work we extend continuous diffusion models to this setting, proposing two complementary approaches. One constructing a reflected Brownian motion as the noising process, and another one based on barrier methods. For both approaches, we derive the time-reversal formula, propose discretisation schemes and extend the score matching toolbox. In practice, we show that reflected type methods, while enjoying less theoretical guarantees than their log-barrier counterparts, are more efficient. We demonstrate the efficiency of our method in two real-world scenarios: conformational modelling and robotic arms.

We conclude by highlighting important future directions. First, the computational cost of the performing the reflection when discretising the reflected Brownian motion is high. Finding numerically efficient approximations of the reflected process is therefore necessary to extend this methodology to very high dimensional settings. Second, the retraction used in place of the exponential map for the barrier method leads to a high number of discretisation steps to ensure a good approximation. Designing faster forward process for the log-barrier method is key to target more complex distributions. Finally, quantum Bayesian applications (Lukens et al., 2020) are a challenging research direction requiring the addition of *sparsity* constraints to our framework.

References

- Ablin, P. and Peyré, G. Fast and accurate optimization on the orthogonal manifold without retraction. In *International Conference on Artificial Intelligence and Statistics*, pp. 5636–5657. PMLR, 2022.
- Bossy, M., Gobet, E., and Talay, D. A symmetrized euler scheme for an efficient approximation of reflected diffusions. *Journal of applied probability*, 41(3):877–889, 2004.
- Boyd, S., Boyd, S. P., and Vandenberghe, L. *Convex optimization*. Cambridge university press, 2004.
- Bradbury, J., Frostig, R., Hawkins, P., Johnson, M. J., Leary, C., Maclaurin, D., Necula, G., Paszke, A., VanderPlas, J., Wanderman-Milne, S., and Zhang, Q. JAX: composable transformations of Python+NumPy programs, 2018. URL <http://github.com/google/jax>.
- Brezis, H. and Brézis, H. *Functional analysis, Sobolev spaces and partial differential equations*, volume 2. Springer, 2011.
- Burdzy, K., Chen, Z.-Q., and Sylvester, J. The heat equation and reflected brownian motion in time-dependent domains. *The Annals of Probability*, 32(1B):775–804, 2004.
- Cattiaux, P., Conforti, G., Gentil, I., and Léonard, C. Time reversal of diffusion processes under a finite entropy condition. *arXiv preprint arXiv:2104.07708*, 2021.
- Claude J. P. Bélisle, Romeijn, H. E., and Smith, R. L. Hit-and-Run Algorithms for Generating Multivariate Distributions. *Mathematics of Operations Research*, 18(2): 255–266, 1993. ISSN 0364765X, 15265471. URL <http://www.jstor.org/stable/3690278>.
- Corso, G., Stärk, H., Jing, B., Barzilay, R., and Jaakkola, T. DiffDock: Diffusion Steps, Twists, and Turns for Molecular Docking, October 2022. URL <http://arxiv.org/abs/2210.01776>.
- De Bortoli, V., Mathieu, E., Hutchinson, M., Thornton, J., Teh, Y. W., and Doucet, A. Riemannian score-based generative modeling, 2022.
- Dhariwal, P. and Nichol, A. Diffusion models beat GAN on image synthesis. *arXiv preprint arXiv:2105.05233*, 2021.
- Dougherty, P. G., Sahni, A., and Pei, D. Understanding cell penetration of cyclic peptides. *Chemical Reviews*, 119(17):10241–10287, 2019.
- Eastman, P., Swails, J., Chodera, J. D., McGibbon, R. T., Zhao, Y., Beauchamp, K. A., Wang, L.-P., Simonnet, A. C., Harrigan, M. P., Stern, C. D., et al. Openmm 7: Rapid development of high performance algorithms for molecular dynamics. *PLoS computational biology*, 13(7): e1005659, 2017.
- Gatmiry, K. and Vempala, S. S. Convergence of the riemannian langevin algorithm. *arXiv preprint arXiv:2204.10818*, 2022.
- Golub, G. H. and Van Loan, C. F. *Matrix computations*. JHU press, 2013.
- Gretton, A., Borgwardt, K. M., Rasch, M. J., Schölkopf, B., and Smola, A. A kernel two-sample test. *Journal of Machine Learning Research*, 13(null):723–773, March 2012. ISSN 1532-4435.
- Han, L. and Rudolph, L. Inverse kinematics for a serial chain with joints under distance constraints. In *Robotics: Science and systems*, 2006.
- Harrison, J. M. and Williams, R. J. Brownian models of open queueing networks with homogeneous customer populations. *Stochastics: An International Journal of Probability and Stochastic Processes*, 22(2):77–115, 1987.
- Hausmann, U. G. and Pardoux, E. Time reversal of diffusions. *The Annals of Probability*, pp. 1188–1205, 1986.
- Heirendt, L., Arreckx, S., Pfau, T., Mendoza, S. N., Richelle, A., Heinken, A., Haraldsdóttir, H. S., Wachowiak, J., Keating, S. M., Vlasov, V., et al. Creation and analysis of biochemical constraint-based models using the cobra toolbox v. 3.0. *Nature protocols*, 14(3):639–702, 2019.
- Ho, J., Jain, A., and Abbeel, P. Denoising diffusion probabilistic models. *Advances in Neural Information Processing Systems*, 2020.
- Hornak, V., Abel, R., Okur, A., Strockbine, B., Roitberg, A., and Simmerling, C. Comparison of multiple amber force fields and development of improved protein backbone parameters. *Proteins: Structure, Function, and Bioinformatics*, 65(3):712–725, 2006.
- Hsu, E. P. *Stochastic analysis on manifolds*. Number 38. American Mathematical Soc., 2002.
- Huang, C.-W., Lim, J. H., and Courville, A. C. A variational perspective on diffusion-based generative models and score matching. *Advances in Neural Information Processing Systems*, 34:22863–22876, 2021.
- Huang, C.-W., Aghajohari, M., Bose, A. J., Panangaden, P., and Courville, A. Riemannian Diffusion Models, August 2022.

- Hyvärinen, A. Estimation of non-normalized statistical models by score matching. *Journal of Machine Learning Research*, 6(4), 2005.
- Ingraham, J., Baranov, M., Costello, Z., Frappier, V., Ismail, A., Tie, S., Wang, W., Xue, V., Obermeyer, F., Beam, A., et al. Illuminating protein space with a programmable generative model. *bioRxiv*, pp. 2022–12, 2022.
- Jaquier, N., Rozo, L., Caldwell, D. G., and Calinon, S. Geometry-aware manipulability learning, tracking, and transfer. *The International Journal of Robotics Research*, 40(2-3):624–650, 2021.
- Jing, B., Corso, G., Chang, J., Barzilay, R., and Jaakkola, T. Torsional Diffusion for Molecular Conformer Generation, June 2022. URL <http://arxiv.org/abs/2206.01729>.
- Jørgensen, E. The central limit problem for geodesic random walks. *Zeitschrift für Wahrscheinlichkeitstheorie und verwandte Gebiete*, 32(1-2):1–64, 1975.
- Kang, W. and Ramanan, K. On the submartingale problem for reflected diffusions in domains with piecewise smooth boundaries. 2017.
- Kannan, R. and Narayanan, H. Random walks on polytopes and an affine interior point method for linear programming. In *Proceedings of the Forty-First Annual ACM Symposium on Theory of Computing*, STOC '09, pp. 561–570, New York, NY, USA, 2009. Association for Computing Machinery. ISBN 9781605585062. doi: 10.1145/1536414.1536491. URL <https://doi.org/10.1145/1536414.1536491>.
- Kingma, D. P. and Ba, J. Adam: A method for stochastic optimization, 2014. URL <http://arxiv.org/abs/1412.6980>.
- Kook, Y., Lee, Y. T., Shen, R., and Vempala, S. S. Sampling with riemannian hamiltonian monte carlo in a constrained space. *arXiv preprint arXiv:2202.01908*, 2022.
- Krivov, S. V. and Karplus, M. Hidden complexity of free energy surfaces for peptide (protein) folding. *Proceedings of the National Academy of Sciences*, 101(41):14766–14770, 2004.
- Lane, T. J. Protein structure prediction has reached the single-structure frontier. *Nature Methods*, pp. 1–4, 2023.
- Leach, A., Schmon, S. M., Degiacomi, M. T., and Willcocks, C. G. Denoising Diffusion Probabilistic Models on SO(3) for Rotational Alignment. *ICLR 2022 Workshop on Geometrical and Topological Representation Learning*, pp. 8, 2022.
- Lee, J. M. Smooth manifolds. In *Introduction to Smooth Manifolds*, pp. 1–31. Springer, 2013.
- Lee, Y. T. and Vempala, S. S. Geodesic walks in polytopes. In *Proceedings of the 49th Annual ACM SIGACT Symposium on Theory of Computing*, pp. 927–940, Montreal Canada, June 2017. ACM. ISBN 978-1-4503-4528-6. doi: 10.1145/3055399.3055416.
- Lee, Y. T. and Vempala, S. S. Convergence rate of riemannian hamiltonian monte carlo and faster polytope volume computation. In *Proceedings of the 50th Annual ACM SIGACT Symposium on Theory of Computing*, pp. 1115–1121, 2018.
- Lewis, N., Nagarajan, H., and Palsson, B. Constraining the metabolic genotype-phenotype relationship using a phylogeny of in silico methods. *Nature Reviews Microbiology*, 10(4):291–305, April 2012. ISSN 1740-1526. doi: 10.1038/nrmicro2737.
- Lions, P.-L. and Sznitman, A.-S. Stochastic differential equations with reflecting boundary conditions. *Communications on pure and applied Mathematics*, 37(4):511–537, 1984.
- Loper, J. Uniform ergodicity for brownian motion in a bounded convex set. *Journal of Theoretical Probability*, 33(1):22–35, 2020.
- Lovász, L. and Vempala, S. Hit-and-run from a corner. *SIAM Journal on Computing*, 35(4):985–1005, 2006. doi: 10.1137/S009753970544727X.
- Lukens, J. M., Law, K. J., Jasra, A., and Lougovski, P. A practical and efficient approach for bayesian quantum state estimation. *New Journal of Physics*, 22(6):063038, 2020.
- Miolane, N., Guigui, N., Brigant, A. L., Mathe, J., Hou, B., Thanwerdas, Y., Heyder, S., Peltre, O., Koep, N., Zaatiti, H., Hajri, H., Cabanes, Y., Gerald, T., Chauchat, P., Shewmake, C., Brooks, D., Kainz, B., Donnat, C., Holmes, S., and Pennec, X. Geomstats: A python package for riemannian geometry in machine learning. *Journal of Machine Learning Research*, 21(223):1–9, 2020. URL <http://jmlr.org/papers/v21/19-027.html>.
- Morris, B. J. Improved bounds for sampling contingency tables. *Random Structures & Algorithms*, 21(2):135–146, 2002. doi: <https://doi.org/10.1002/rsa.10049>. URL <https://onlinelibrary.wiley.com/doi/abs/10.1002/rsa.10049>.
- Nesterov, Y. et al. *Lectures on convex optimization*, volume 137. Springer, 2018.

- Noble, M., De Bortoli, V., and Durmus, A. Barrier Hamiltonian Monte Carlo, October 2022.
- Pacchiarotti, B., Costantini, C., and Sartoretto, F. Numerical approximation for functionals of reflecting diffusion processes. *SIAM Journal on Applied Mathematics*, 58(1): 73–102, 1998.
- Petit, F. Time reversal and reflected diffusions. *Stochastic Processes and their Applications*, 69(1):25–53, July 1997. ISSN 03044149. doi: 10.1016/S0304-4149(97)00035-5.
- Revuz, D. and Yor, M. *Continuous martingales and Brownian motion*, volume 293. Springer Science & Business Media, 2013.
- Rotkiewicz, P. and Skolnick, J. Fast procedure for reconstruction of full-atom protein models from reduced representations. *Journal of computational chemistry*, 29(9): 1460–1465, 2008.
- Saloff-Coste, L. Precise estimates on the rate at which certain diffusions tend to equilibrium. *Mathematische Zeitschrift*, 217(1):641–677, 1994.
- Shkolnikov, M. and Karatzas, I. Time-reversal of reflected Brownian motions in the orthant, July 2013. URL <http://arxiv.org/abs/1307.4422>.
- Skorokhod, A. V. Stochastic equations for diffusion processes in a bounded region. *Theory of Probability & Its Applications*, 6(3):264–274, 1961.
- Smith, R. L. Efficient Monte Carlo Procedures for Generating Points Uniformly Distributed over Bounded Regions. *Operations Research*, 32(6):1296–1308, December 1984. doi: 10.1287/opre.32.6.1296. URL <https://ideas.repec.org/a/inm/ropropre/v32y1984i6p1296-1308.html>.
- Sohl-Dickstein, J., Weiss, E., Maheswaranathan, N., and Ganguli, S. Deep unsupervised learning using nonequilibrium thermodynamics. In *International Conference on Machine Learning*, pp. 2256–2265. PMLR, 2015.
- Song, Y. and Ermon, S. Generative modeling by estimating gradients of the data distribution. In *Advances in Neural Information Processing Systems*, 2019.
- Song, Y., Sohl-Dickstein, J., Kingma, D. P., Kumar, A., Ermon, S., and Poole, B. Score-based generative modeling through stochastic differential equations. In *International Conference on Learning Representations*, 2021.
- Thiele, I., Swainston, N., Fleming, R., Hoppe, A., Sahoo, S., Aurich, M., Haraldsdottir, H., Mo, M., Rolfsson, O., Stobbe, M., Thorleifsson, S., Agren, R., Bölling, C., Bordel, S., Chavali, A., Dobson, P., Dunn, W., Endler, L., Hala, D., Hucka, M., Hull, D., Jameson, D., Jamshidi, N., Jonsson, J., Juty, N., Keating, S., Nookaew, I., Le Novère, N., Malys, N., Mazein, A., Papin, J., Price, N., Selkov, E., Sigurdsson, M., Simeonidis, E., Sonnenschein, N., Smallbone, K., Sorokin, A., van Beek, J., Weichart, D., Goryanin, I., Nielsen, J., Westerhoff, H., Kell, D., Mendes, P., and Palsson, B. A community-driven global reconstruction of human metabolism. *Nature Biotechnology*, March 2013. ISSN 1087-0156. doi: 10.1038/nbt.2488.
- Trippe, B. L., Yim, J., Tischler, D., Broderick, T., Baker, D., Barzilay, R., and Jaakkola, T. Diffusion probabilistic modeling of protein backbones in 3D for the motif-scaffolding problem, June 2022.
- Urain, J., Funk, N., Chalvatzaki, G., and Peters, J. Se(3)-diffusionfields: Learning cost functions for joint grasp and motion optimization through diffusion. *arXiv preprint arXiv:2209.03855*, 2022.
- Vincent, P. A connection between score matching and denoising autoencoders. *Neural Computation*, 23(7):1661–1674, 2011.
- Watson, J. L., Juergens, D., Bennett, N. R., Trippe, B. L., Yim, J., Eisenach, H. E., Ahern, W., Borst, A. J., Ragotte, R. J., Milles, L. F., Wicky, B. I. M., Hanikel, N., Pellock, S. J., Courbet, A., Sheffler, W., Wang, J., Venkatesh, P., Sappington, I., Torres, S. V., Lauko, A., Bortoli, V. D., Mathieu, E., Barzilay, R., Jaakkola, T. S., DiMaio, F., Baek, M., and Baker, D. Broadly applicable and accurate protein design by integrating structure prediction networks and diffusion generative models, December 2022.
- Williams, R. J. Reflected Brownian motion with skew symmetric data in a polyhedral domain. *Probability Theory and Related Fields*, 75(4):459–485, August 1987. ISSN 0178-8051, 1432-2064. doi: 10.1007/BF00320328.
- Wu, K. E., Yang, K. K., Berg, R. v. d., Zou, J. Y., Lu, A. X., and Amini, A. P. Protein structure generation via folding diffusion. *arXiv preprint arXiv:2209.15611*, 2022.
- Yoshikawa, T. Manipulability of robotic mechanisms. *The international journal of Robotics Research*, 4(2):3–9, 1985.

A. Introduction

In this supplementary, we first recall some key concepts from Riemannian geometry in Appendix B. In Appendix C we remind the expression of the Brownian motion in local coordinates, and use it to derive the SDE that the Langevin dynamics satisfy. In Appendix D we derive the implicit score matching loss. We give details about the likelihood evaluation in Appendix E. Then in Appendix G we prove the time-reversal formula of reflected Brownian motion. In Appendix H we give some background on the conformational modelling of proteins backbone for the experiment in Section 5.3. In Appendix I we detail the geometrical constraint arising from the configurational robotics arm modelling experiment from Section 5.2. Additional results, training and miscellaneous experimental details are reported in Appendix J.

B. Manifold concepts

For readers unfamiliar with Riemannian geometry here we give a brief overview of some of the key concepts. This is not a technical introduction, but a conceptual one for the understanding of terms. For a technical introduction, we refer readers to Lee (2013). A Riemannian manifold is a tuple $(\mathcal{M}, \mathfrak{g})$ with \mathcal{M} a smooth manifold and \mathfrak{g} a metric which defines an inner product on tangent spaces.

A *smooth manifold* is a topological space which locally can be described by Euclidean space. It is characterised by a family of *charts* $\{U \subset \mathcal{M}, \phi : U \rightarrow \mathbb{R}^d\}$, homeomorphic mappings between subsets of the manifold and Euclidean space. The collection of charts must cover the whole manifold. For the manifolds to be smooth the charts must be smooth, and the transition between charts where their domains overlap must also be smooth.

The *metric* on a Riemannian manifold gives the manifold a notion of distance and curvature. The same underlying smooth manifold with different metrics can look wildly different. The metric is defined as a smooth choice of positive definite inner product on each of the tangent spaces of the manifold. That is we have at every point a symmetric bilinear map

$$\mathfrak{g}(p) : T_p\mathcal{M} \times T_p\mathcal{M} \rightarrow \mathbb{R}$$

The tangent space of a point on a manifold is the generalisation of the notion of tangent planes and can be thought of as the space of derivatives of scalar functions on the manifold at that point. The collection of all tangent spaces is written as $T\mathcal{M} = \bigcup_{p \in \mathcal{M}} T_p\mathcal{M}$ and is called the tangent bundle. It is also manifold. Vector fields on manifolds are defined by making a choice of tangent vector at every point on the manifold in a smooth fashion. The space of vector fields is written as $\Gamma(T\mathcal{M})$ and is more technically the space of *sections* of the tangent bundle.

One thing that the metric itself does not immediately define is how different tangent spaces at points on the manifold relate to one another. For this, we need additionally the concept of a *connection*. A connection is a map that takes two vector fields and produces a derivative of the first with respect to the second, that is a function $\nabla : \Gamma(T\mathcal{M}) \times \Gamma(T\mathcal{M}) \rightarrow \Gamma(T\mathcal{M})$ and it typically written as $\nabla(X, Y) = \nabla_X Y$. Such a connection must for $X, Y, Z \in \Gamma(T\mathcal{M})$ and smooth functions on the manifold $a, b : \mathcal{M} \rightarrow \mathbb{R}$ obey the following conditions:

- (a) $\nabla_{aX+bY} Z = a\nabla_X Z + b\nabla_Y Z$,
- (b) $\nabla_X(Y + Z) = \nabla_X Y + \nabla_X Z$,
- (c) $\nabla_X(aY) = \partial_X a Y + a\nabla_X Y$,

where $\partial_X a Y$ is the regular *directional derivative* of aY in the direction X . These conditions ensure the connection is a well-defined derivative. In what follows, we focus on a specific choice of connection which is particularly well-suited for Riemannian manifolds.

On a given manifold, there are infinitely many connections. Fortunately, there is a natural choice, called the *Levi-Civita* connection if we impose two additional conditions:

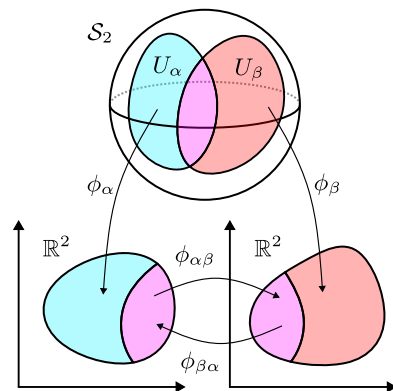


Figure 10: Example charts of the 2D manifold S^2 .

- (a) $X \cdot (\mathbf{g}(Y, Z)) = \mathbf{g}(\nabla_X Y, Z) + \mathbf{g}(Y, \nabla_X Z)$,
 (b) $[X, Y] = \nabla_X Y - \nabla_Y X$,

where $[\cdot, \cdot]$ is the Lie bracket. The first condition ensures that the metric is preserved by the connection. That is to say, the *parallel transport* (to be defined shortly) using the connection leaves inner products unchanged on the manifold. The second ensures the connection is *torsion-free*. The change in tangent space along a geodesic (again to be defined shortly) can be described in two parts, the *curvature*, how the tangent space rotates perpendicular to the direction of travel, and the torsion, how the tangent space rotates around the axis of the direction of travel. The curvature of the connection is uniquely fixed by the other 4 conditions (the well-defined derivative and preservation of the metric). The torsion however is not fixed. By requiring it to be zero we ensure a unique connection. The requirement of zero torsion also has implications for ensuring integrability on the manifold.

With the metric and the Levi-Cevita connection in hand, we can define a number of key concepts.

We say that a vector field X is *parallel* to a curve $\gamma : (0, 1) \rightarrow \mathcal{M}$ if

$$\nabla_{\gamma'} X = 0$$

where $\gamma' : (0, 1) \rightarrow T_{\gamma(t)}\mathcal{M}$ is the derivative of the path. For two points on the manifold $p, q \in \mathcal{M}$ and a curve between them, $\gamma, \gamma(0) = p, \gamma(1) = q$, for an initial vector $X_0 \in T_p\mathcal{M}$ there is a unique vector field X that is parallel to γ such that $X(p) = X_0$. This induces a map between the tangent spaces at p and q

$$\tau_\gamma : T_p\mathcal{M} \rightarrow T_q\mathcal{M}$$

This map is referred to as the *parallel transport* of tangent vectors between p and q , and this satisfies the condition that for $\mathbf{v}, \mathbf{u} \in T_p\mathcal{M}$

$$\mathbf{g}(p)(\mathbf{v}, \mathbf{u}) = \mathbf{g}(q)(\tau_\gamma(\mathbf{v}), \tau_\gamma(\mathbf{u})).$$

A *geodesic* on a manifold is the unique path on the manifold $\gamma : (0, 1) \rightarrow \mathcal{M}$ such that $\nabla_{\gamma'} \gamma' = 0$. It is also the shortest path between two points on a manifold in the sense that

$$L(\gamma) = \int_0^1 \sqrt{\mathbf{g}(\gamma'(t), \gamma'(t))} dt,$$

is minimal out of any path between the start and end of the geodesic. Geodesics give the notion of ‘straight lines’ on manifolds. We define the *exponential map* on a manifold as the mapping between an element of the tangent space at point p , $\mathbf{v} \in T_p\mathcal{M}$ and the endpoint of the unique geodesic γ with $\gamma(0) = p$ and $\gamma'(0) = \mathbf{v}$. In the tangent space of a manifold, we require the notion of a reflection in order to reflect geodesics off of boundary constraints. If at a point in the manifold with have $\mathbf{v} \in T_p\mathcal{M}$ and a unit vector normal to the constraint $\mathbf{n} \in T_p\mathcal{M}$, then the reflection of this vector is given by $\mathbf{v}' = \mathbf{v} - 2\mathbf{g}(\mathbf{v}, \mathbf{n})\mathbf{n}$.

C. Brownian motion in local coordinates

We consider a smooth function $f \in C^\infty(\mathcal{M})$. The Laplace-Beltrami operator $\Delta_{\mathcal{M}}$ is given by $\Delta_{\mathcal{M}}(f) = \text{div}(\text{grad}(f))$. In local coordinates we have

$$\text{div}(X) = (\det(\mathbf{g})^{-1/2}) \sum_{i=1}^d \partial_i (\det(\mathbf{g})^{1/2} X_i),$$

as well as

$$\text{grad}(f) = \mathbf{g}^{-1} \nabla f.$$

Therefore, the Laplace-Beltrami operator is given by

$$\Delta_{\mathcal{M}}(f) = \sum_{i,j=1}^d \mathbf{g}_{i,j}^{-1} \partial_{i,j} f + (\det(\mathbf{g})^{-1/2}) \sum_{i,j=1}^d \partial_i (\det(\mathbf{g})^{1/2} \mathbf{g}_{i,j}^{-1}) \partial_j f.$$

Therefore, in local coordinates the infinitesimal generator associated with the Laplace-Beltrami operator is given by

$$\mathcal{A}(f) = \sum_{i,j=1}^d \mathbf{g}_{i,j}^{-1} \partial_{i,j} f + \langle b^i, \nabla f \rangle,$$

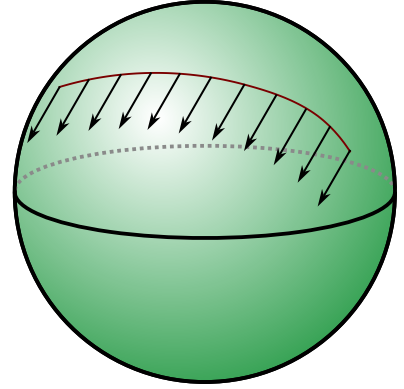


Figure 11: Parallel transport of vectors along a path on the sphere.

with

$$b^i = (\det(\mathbf{g})^{-1/2}) \sum_{j=1}^d \partial_j (\det(\mathbf{g})^{1/2} \mathbf{g}_{i,j}^{-1}). \quad (10)$$

Therefore, the dual operator associated with \mathcal{A} is given by

$$\mathcal{A}^*(f) = \sum_{i,j=1}^d \partial_{i,j} (\mathbf{g}_{i,j}^{-1} f) - \sum_{i=1}^d \partial_i (b^i f).$$

Note that by letting $f = \det(\mathbf{g})^{1/2}$ we get that $\mathcal{A}^*(f) = 0$ and therefore we recover that $p \propto \det(\mathbf{g})$ is the invariant distribution of the Brownian motion.

Langevin dynamics on \mathcal{M} . We know that the Brownian motion targets $\det(\mathbf{g})^{1/2}$. Therefore in order to correct and sample from the uniform distribution we consider the Langevin dynamics

$$d\mathbf{X}_t = -\text{grad} \log(\det(\mathbf{g})^{1/2})(\mathbf{X}_t) dt + \sqrt{2} d\mathbf{B}_t^{\mathcal{M}}.$$

Note that in the previous equation grad and $\mathbf{B}_t^{\mathcal{M}}$ are defined w.r.t. the metric of the manifold. In local coordinates we have

$$d\mathbf{X}_t = \{b - \text{grad} \log(\det(\mathbf{g})^{1/2})\}(\mathbf{X}_t) dt + \sqrt{2} \mathbf{g}(\mathbf{X}_t)^{-1/2} d\mathbf{B}_t. \quad (11)$$

where $b = \{b^i\}_{i=1}^d$ is given in (10). In addition, we have

$$\text{grad} \log(\det(\mathbf{g})^{1/2}) = \det(\mathbf{g})^{-1/2} \mathbf{g}^{-1} \nabla \det(\mathbf{g}). \quad (12)$$

Using (10) we have

$$b^i = (\det(\mathbf{g})^{-1/2}) \sum_{j=1}^d \partial_j (\det(\mathbf{g})^{1/2} \mathbf{g}_{i,j}^{-1}) = \sum_{j=1}^d \partial_j \mathbf{g}_{i,j}^{-1} + \text{grad} \log(\det(\mathbf{g})^{1/2})_i$$

This can also be rewritten as

$$\text{div}_{\mathcal{M}}(\mathbf{g}^{-1}) = \mu + \text{grad} \log(\det(\mathbf{g})^{1/2}),$$

with

$$\mu_i = \sum_{j=1}^d \partial_j \mathbf{g}_{i,j}^{-1}.$$

Combining this result and (12) we get that (11) can be rewritten as

$$d\mathbf{X}_t = \mu(\mathbf{X}_t) + \sqrt{2} d\mathbf{B}_t.$$

Note that (up to a factor 2) this is the same SDE as the one considered in [Lee & Vempala \(2017\)](#).

D. Implicit Score Matching Loss

Using the divergence theorem, we have

$$\begin{aligned} & (1/2) \int_{\mathcal{M}} \|\mathbf{s}_{\theta}(x) - \nabla \log p_t(x)\|^2 p_t(x) d\mu(x) \\ &= (1/2) \int_{\mathcal{M}} \|\mathbf{s}_{\theta}(x)\|^2 p_t(x) d\mu(x) - \int_{\mathcal{M}} \langle \mathbf{s}_{\theta}(x), \nabla \log p_t(x) \rangle p_t(x) d\mu(x) + (1/2) \int_{\mathcal{M}} \|\nabla \log p_t(x)\|^2 p_t(x) d\mu(x) \\ &= (1/2) \int_{\mathcal{M}} \|\mathbf{s}_{\theta}(x)\|^2 p_t(x) d\mu(x) - \int_{\partial \mathcal{M}} \langle \mathbf{s}_{\theta}(x), \mathbf{n} \rangle p_t(x) d\nu(x) \\ & \quad + \int_{\mathcal{M}} \text{div}(\mathbf{s}_{\theta})(x) p_t(x) d\mu(x) + (1/2) \int_{\mathcal{M}} \|\nabla \log p_t(x)\|^2 p_t(x) d\mu(x). \end{aligned}$$

Using that $\mathbf{s}_{\theta}(x) = 0$ for all $x \in \partial \mathcal{M}$, we get that

$$\begin{aligned} & (1/2) \int_{\mathcal{M}} \|\mathbf{s}_{\theta}(x) - \nabla \log p_t(x)\|^2 p_t(x) d\mu(x) \\ &= (1/2) \int_{\mathcal{M}} \|\mathbf{s}_{\theta}(x)\|^2 p_t(x) d\mu(x) + \int_{\mathcal{M}} \text{div}(\mathbf{s}_{\theta})(x) p_t(x) d\mu(x) + (1/2) \int_{\mathcal{M}} \|\nabla \log p_t(x)\|^2 p_t(x) d\mu(x), \end{aligned}$$

which concludes the proof.

E. Likelihood evaluation

One main advantage of constructing a continuous noising process, is that similarly to [Song et al. \(2021\)](#), we can evaluate the model's likelihood via the following *probability flow* Ordinary Differential Equation (ODE). In particular for the Langevin dynamics Equation (5) which we recall

$$d\mathbf{X}_t = \frac{1}{2}\text{div}(\mathbf{g}^{-1})(\mathbf{X}_t)dt + \mathbf{g}(\mathbf{X}_t)^{-\frac{1}{2}}d\mathbf{B}_t,$$

the following ODE has the same marginal density

$$d\mathbf{Y}_t = \left[\frac{1}{2}\nabla \cdot \mathbf{g}^{-1}(\mathbf{Y}_t) - \frac{1}{2}\mathbf{g}^{-1}(\mathbf{Y}_t)\nabla \log p_t(\mathbf{Y}_t) \right] dt.$$

F. Reflected Brownian Motion and Skorokhod problems

In this section, we provide the basic definitions and results to derive the time-reversal of the reflected Brownian motion in Appendix G. We follow closely the presentation of [Lions & Sznitman, 1984](#)) and [Burdzy et al., 2004](#)). We first define the *Skorokhod problem* for deterministic problems. We consider \mathcal{M} to be a smooth open bounded domain. We recall that the normal vector n is defined on $\partial\mathcal{M}$ and we set $n(x) = 0$ for any $x \notin \partial\mathcal{M}$.

Before giving the definition of the *Skorokhod problem*, we recall what is the space of functions of *bounded variations*.

Definition F.1. Let $a, b \in (-\infty, +\infty)$ and $f : \in C([a, b], \mathbb{R})$. We define the *total variation* of f as

$$V_{a,b}(f) = \sup\{\sum_{i=0}^{n-1} \|f(x_{i+1}) - f(x_i)\| : (x_i)_{i=0}^{n-1}, a = x_0 \leq x_1 \leq \dots \leq x_{n-1} \leq x_n = b, n \in \mathbb{N}\}.$$

f has bounded variations over $[a, b]$ if $V_{a,b}(f) < +\infty$. Let $f \in C([0, +\infty), \mathbb{R})$. f has bounded variations over $[0, +\infty)$ if for any $b > 0$, f has bounded variations over $[0, b]$.

The notion of bounded variation is a relaxation of the differentiability requirement. In particular, if $f \in C^1([a, b], \mathbb{R})$, we have $V_{a,b}(f) = \int_a^b \|f'(t)\| dt$. In the definition of the *Skorokhod problem*, we will see that this relaxation is necessary, even in the deterministic setting.

For any function of bounded variation $f \in C([a, b], \mathbb{R})$ on $[a, b]$, we define $|f| : [a, b] \rightarrow [0, +\infty)$ given for any $t \in [a, b]$ by $|f|_t = V_{a,t}(f)$. Note that $|f|$ is non-decreasing and right-continuous. Therefore, we can define the measure $\mu_{|f|}$ on $[a, b]$, given for any $s, t \in [a, b]$ with $t \geq s$ by $\mu_{|f|}([s, t]) = |f|(t) - |f|(s)$. In particular, for any $\varphi : [a, b] \rightarrow \mathbb{R}_+$, we define

$$\int_a^b \varphi(t) d|f|_t = \int_a^b \varphi(t) d\mu_{|f|}(t).$$

In addition, f can be decomposed in a difference of two non-decreasing processes right continuous processes g_1, g_2 , where for any $t \in [a, b]$, $f(t) = g_1(t) - g_2(t)$, $g_1(t) = |f|_t$ and $g_2(t) = |f|_t - f(t)$. Hence, for every φ bounded on $[a, b]$, we can define

$$\int_a^b \varphi(t) df(t) = \int_a^b \varphi(t) dg_1(t) - \int_a^b \varphi(t) dg_2(t).$$

Note that these definitions can be extended to the setting where $f : [a, b] \rightarrow \mathbb{R}^d$.

We begin with the following result, see [Lions & Sznitman, 1984](#)).

Theorem F.2. Let $(x_t)_{t \geq 0} \in C([0, +\infty), \mathbb{R})$. Then, there exists a unique couple $(\bar{x}_t, k_t)_{t \geq 0}$ such that

- (a) $(k_t)_{t \geq 0}$ has bounded variation over $[0, +\infty)$.
- (b) $(\bar{x}_t)_{t \geq 0} \in C([0, +\infty), \overline{\mathcal{M}})$.
- (c) For any $t \geq 0$, $x_t + k_t = \bar{x}_t$.
- (d) For any $t \geq 0$, $|k|_t = \int_0^t \mathbf{1}_{\bar{x}_s \in \partial\mathcal{M}}(\bar{x}_s) d|k|_s$ and $k_t = \int_0^t n(\bar{x}_s) d|k|_s$.

Let us discuss Theorem F.2. First, Theorem F.2-(c) states the original (unconstrained) process $(x_t)_{t \geq 0}$ can be decomposed into a constrained version $(\bar{x}_t)_{t \geq 0}$ and a bounded variation process $(k_t)_{t \geq 0}$. The process $(|k|_t)_{t \geq 0}$ counts the number of

times the constrained process $(\bar{x}_t)_{t \geq 0}$ hits the boundary. More formally, we have $|k|_t = \int_0^t \mathbf{1}_{x \in \partial \mathcal{M}}(\bar{x}_s) d|k|_s$. When, we hit the boundary, we reflect the process. This condition is expressed in $k_t = \int_0^t n(\bar{x}_s) d|k|_s$.

We now consider the extension to stochastic processes. We are given $(\mathbf{X}_t)_{t \geq 0}$ such that

$$d\mathbf{X}_t = b(\mathbf{X}_t)dt + \sigma(t)d\mathbf{B}_t,$$

where $(\mathbf{B}_t)_{t \geq 0}$ is a d -dimensional Brownian motion. We also assume that b and σ are Lipschitz which implies the existence and strong uniqueness of $(\mathbf{X}_t)_{t \geq 0}$. We have the following result (Lions & Sznitman, 1984).

Theorem F.3. *There exists a unique process $(\bar{\mathbf{X}}_t, \mathbf{k}_t)_{t \geq 0}$ such that*

- (a) $(\mathbf{k}_t)_{t \geq 0}$ has bounded variation over $[0, +\infty)$ almost surely.
- (b) $(\bar{\mathbf{X}}_t)_{t \geq 0} \in C([0, +\infty), \bar{\mathcal{M}})$.
- (c) For any $t \geq 0$, $\bar{\mathbf{X}}_t = \bar{\mathbf{X}}_0 + \int_0^t b(\bar{\mathbf{X}}_s)ds + \int_0^t \sigma(\bar{\mathbf{X}}_s)d\mathbf{B}_s - \mathbf{k}_t$.
- (d) For any $t \geq 0$, $|k|_t = \int_0^t \mathbf{1}_{\bar{x}_s \in \partial \mathcal{M}}(\bar{x}_s) d|k|_s$ and $\mathbf{k}_t = \int_0^t n(\bar{x}_s) d|k|_s$.

The process $(\mathbf{X}_t)_{t \geq 0}$ is almost surely continuous, so we could apply the previous theorem almost surely for all the realizations of the process. However, this does not tell us if the obtained solutions $(\bar{\mathbf{X}}_t, \mathbf{k}_t)_{t \geq 0}$ form themselves a process. The main difference with Theorem F.2 is in Theorem F.3-(c) which differs from Theorem F.3-(c). Note that in the case where $b = 0$ and $\sigma = \text{Id}$ we recover Theorem F.3-(c). This is not true in the general case. However, it can be seen that for any realization of the process $(\bar{\mathbf{X}}_t)_{t \geq 0}$, we have that $(\bar{\mathbf{X}}_t, \mathbf{k}_t)_{t \geq 0}$ is solution of the *deterministic* Skorokhod problem by letting $x_t = \bar{\mathbf{X}}_0 + \int_0^t b(\bar{\mathbf{X}}_s)ds + \int_0^t \sigma(\bar{\mathbf{X}}_s)d\mathbf{B}_s$. The backward and forward Kolmogorov equations can be found in (Burdzy et al., 2004). Note that the presence of the process $(\mathbf{k}_t)_{t \geq 0}$ incurs notable complications compared to unconstrained processes. In particular, there is no martingale problem associated with weak solutions of reflected SDEs but only sub-martingale problems, see (Kang & Ramanan, 2017) for instance.

G. Time-reversal for reflected Brownian motion

We start with the following definition.

Definition G.1. Let $\mathcal{M} \subset \mathbb{R}^d$ be an open set. \mathcal{M} has a smooth boundary if for any $x \in \partial \mathcal{M}$, there exists $U \subset \mathbb{R}^d$ open and $f \in C^\infty(U, \mathbb{R})$ such that $x \in U$ and (a) $\text{cl}(\mathcal{M}) \cap U = \{x \in U : f(x) \leq 0\}$, (b) $\nabla f(x) \neq 0$ for any $x \in U$ where $\text{cl}(\mathcal{M})$ is the closure of \mathcal{M} .

We will make the use of the following lemma which is a straightforward extension of Burdzy et al. (2004, Theorem 2.6).

Lemma G.2. *Let u such that $s \mapsto u(s, x) \in C^1((0, T), \mathbb{R})$, for any $s \in (0, T)$, $x \mapsto u(s, x) \in C^2(\mathcal{M}, \mathbb{R})$ and $u \in C^1(\text{cl}(\mathcal{M}), \mathbb{R})$. Then for any $T \geq 0$, $s, t \in [0, T]$, we have*

$$\mathbb{E}[\int_s^t u(w, \bar{\mathbf{B}}_w) d\mathbf{k}_w] = \frac{1}{2} \int_s^t \int_{\partial \mathcal{M}} u(w, x) p_w(x) d\sigma(x) dw.$$

Note that we recover Burdzy et al. (2004, Theorem 2.6) if we set $u = 1$. We also emphasize that the result of Burdzy et al. (2004, Theorem 2.6) is stronger than Theorem G.2 as it holds not only in expectation but also in L^2 and almost surely.

We are now ready to prove Theorem 3.2. We follow the approach of (Petit, 1997) which itself is based on an extension of (Haussmann & Pardoux, 1986). We refer to Cattiaux et al. (2021) for recent entropic approaches of time-reversal. Recall that $(\bar{\mathbf{B}}_t, \mathbf{k}_t)_{t \geq 0}$ is a solution to the Skorokhod problem (Skorokhod, 1961) if $(\mathbf{k}_t)_{t \geq 0}$ is a bounded variation process and $(\bar{\mathbf{B}}_t)_{t \geq 0}$ a continuous adapted process such that for any $t \geq 0$, $\mathbf{B}_t = \bar{\mathbf{B}}_t + \mathbf{k}_t \in \mathcal{M}$, $(\bar{\mathbf{B}}_t)_{t \geq 0}$ and

$$|\mathbf{k}|_t = \int_0^t \mathbf{1}_{\bar{\mathbf{B}}_s \in \partial \mathcal{M}} d|\mathbf{k}|_s, \quad \mathbf{k}_t = \int_0^t \mathbf{n}(\bar{\mathbf{B}}_s) d|\mathbf{k}|_s, \quad (13)$$

In what follows, we define $(\mathbf{Y}_t)_{t \in [0, T]}$ such that for any $t \in [0, T]$, $\mathbf{Y}_t = \bar{\mathbf{B}}_{T-t}$. Let us consider the process $(\tilde{\mathbf{B}}_t)_{t \in [0, T]}$ defined for any $t \in [0, T]$ by

$$\tilde{\mathbf{B}}_t = -\bar{\mathbf{B}}_T + \bar{\mathbf{B}}_{T-t} + \mathbf{k}_T - \mathbf{k}_{T-t} - \int_{T-t}^T \nabla \log p_s(\bar{\mathbf{B}}_s) ds.$$

First, note that $t \mapsto \bar{\mathbf{B}}_t$ is continuous. Denote by \mathcal{F} , the filtration associated with $(\bar{\mathbf{B}}_{T-t})_{t \in [0, T]}$. We have that $(\bar{\mathbf{B}}_t)_{t \in [0, T]}$ is adapted to $(\bar{\mathbf{B}}_{T-t})_{t \in [0, T]}$. Even more so, we have that $(\bar{\mathbf{B}}_t)_{t \in [0, T]}$ satisfies the strong Markov property since $(\bar{\mathbf{B}}_t)_{t \in [0, T]}$ also satisfies the strong Markov property. Let $g \in C_c^\infty(\text{cl}(\mathcal{M}))$ and consider for any $0 \leq s \leq t \leq T$, $\mathbb{E}[(\bar{\mathbf{B}}_t - \bar{\mathbf{B}}_s)g(\bar{\mathbf{B}}_{T-t})]$. For any $0 \leq s \leq t \leq T$ we have

$$\mathbb{E}[(\bar{\mathbf{B}}_t - \bar{\mathbf{B}}_s)g(\bar{\mathbf{B}}_{T-t})] = \mathbb{E}[(-\bar{\mathbf{B}}_{T-s} + \bar{\mathbf{B}}_{T-t} + \mathbf{k}_{T-s} - \mathbf{k}_{T-t} - \int_{T-t}^{T-s} \nabla \log p_u(\bar{\mathbf{B}}_u) du)g(\bar{\mathbf{B}}_{T-t})]. \quad (14)$$

In what follows, we prove that for any $0 \leq s \leq t \leq T$ we have $\mathbb{E}[(\bar{\mathbf{B}}_t - \bar{\mathbf{B}}_s)g(\bar{\mathbf{B}}_{T-t})] = 0$. Therefore, we only need to prove that for any $0 \leq s \leq t \leq T$ we have

$$\mathbb{E}[(-\bar{\mathbf{B}}_t + \bar{\mathbf{B}}_s + \mathbf{k}_t - \mathbf{k}_s - \int_s^t \nabla \log p_u(\bar{\mathbf{B}}_u) du)g(\bar{\mathbf{B}}_t)] = 0. \quad (15)$$

Let $t \in (0, T]$. We introduce $u : [0, t] \times \mathcal{M}$ such that for any $s \in [0, t]$ and $x \in \mathcal{M}$, $u(s, x) = \mathbb{E}[g(\bar{\mathbf{B}}_t) | \bar{\mathbf{B}}_s = x]$. Using [Burdzy et al. \(2004, Theorem 2.8\)](#) we get that for any $x \in \mathcal{M}$, $s \mapsto u(s, x) \in C^1((0, t), \mathbb{R})$ and for any $s \in (0, t)$, $x \mapsto u(s, x) \in C^2(\mathcal{M}, \mathbb{R})$ and $x \mapsto u(s, x) \in C^1(\text{cl}(\mathcal{M}), \mathbb{R})$. In addition, we have that for any $s \in (0, t)$ and for any $x \in \mathcal{M}$ and $x_0 \in \partial\mathcal{M}$

$$\partial_s u(s, x) + \frac{1}{2} \Delta u(s, x) = 0, \quad \langle \nabla u(s, x_0), \mathbf{n}(x_0) \rangle = 0. \quad (16)$$

This equation is called the backward Kolmogorov equation (note that in the case of a bounded domain, the solutions satisfy the Neumann boundary conditions). Using (16), $\bar{\mathbf{B}}_t = \mathbf{B}_t - \mathbf{k}_t$ for any $t \geq 0$ and the Itô formula for semimartingale ([Revuz & Yor, 2013, Chapter IV, Theorem 3.3](#)) we have that for any $s \in (0, t)$

$$\begin{aligned} \mathbb{E}[u(t, \bar{\mathbf{B}}_t) \bar{\mathbf{B}}_t] &= \mathbb{E}[u(s, \bar{\mathbf{B}}_s) \bar{\mathbf{B}}_s] + \mathbb{E}[\frac{1}{2} \int_s^t \bar{\mathbf{B}}_w \Delta u(w, \bar{\mathbf{B}}_w) dw] + \mathbb{E}[\int_s^t \nabla u(w, \bar{\mathbf{B}}_w) dw] \\ &\quad - \mathbb{E}[\int_s^t \bar{\mathbf{B}}_w \langle \nabla u(w, \bar{\mathbf{B}}_w), \mathbf{n}(\bar{\mathbf{B}}_w) \rangle d|\mathbf{k}|_w] \\ &\quad - \mathbb{E}[\int_s^t u(w, \bar{\mathbf{B}}_w) \mathbf{n}(\bar{\mathbf{B}}_w) d|\mathbf{k}|_w] \\ &\quad + \mathbb{E}[\int_s^t \bar{\mathbf{B}}_w \partial_w u(w, \bar{\mathbf{B}}_w) dw] \\ &= \mathbb{E}[u(s, \bar{\mathbf{B}}_s) \bar{\mathbf{B}}_s] + \mathbb{E}[\int_s^t \nabla u(w, \bar{\mathbf{B}}_w) dw] - \mathbb{E}[\int_s^t u(w, \bar{\mathbf{B}}_w) \mathbf{n}(\bar{\mathbf{B}}_w) d|\mathbf{k}|_w]. \end{aligned} \quad (17)$$

In addition, using the Fubini theorem and the definition of \mathbf{k}_t we have that for any $s \in (0, t)$

$$\mathbb{E}[\int_s^t u(w, \bar{\mathbf{B}}_w) \mathbf{n}(\bar{\mathbf{B}}_w) d|\mathbf{k}|_w] = \mathbb{E}[\int_s^t \mathbb{E}[g(\bar{\mathbf{B}}_t) | \bar{\mathbf{B}}_w] \mathbf{n}(\bar{\mathbf{B}}_w) d|\mathbf{k}|_w] = \mathbb{E}[g(\bar{\mathbf{B}}_t) (\mathbf{k}_t - \mathbf{k}_s)]. \quad (18)$$

Finally, using the divergence theorem and [Burdzy et al. \(2004, Theorem 2.6\)](#) we have that for any $s \in (0, t)$

$$\begin{aligned} \mathbb{E}[\int_s^t \nabla u(w, \bar{\mathbf{B}}_w) dw] &= \int_s^t \int_{\mathcal{M}} \nabla u(w, x) p_w(x) dx dw \\ &= - \int_s^t \int_{\mathcal{M}} u(w, x) \nabla \log(p_w(x)) p_w(x) dx dw + \int_s^t \int_{\partial\mathcal{M}} u(w, x) p_w(x) dx d\sigma(w), \end{aligned}$$

where σ is the surface area measure on $\partial\mathcal{M}$, see [Burdzy et al. \(2004\)](#). Using [Theorem G.2](#) and the Fubini theorem we get that

$$\begin{aligned} \mathbb{E}[\int_s^t \nabla u(w, \bar{\mathbf{B}}_w) dw] &= - \int_s^t \int_{\mathcal{M}} u(w, x) \nabla \log(p_w(x)) p_w(x) dx dw + \mathbb{E}[\int_s^t u(w, \bar{\mathbf{B}}_w) d\mathbf{k}_w] \\ &= - \mathbb{E}[\int_s^t g(\bar{\mathbf{B}}_t) \nabla \log(p_w(\bar{\mathbf{B}}_w)) dw] + 2\mathbb{E}[g(\bar{\mathbf{B}}_t) (\mathbf{k}_t - \mathbf{k}_s)] \end{aligned} \quad (19)$$

Combining (17), (18) and (19) we get that

$$\mathbb{E}[u(t, \bar{\mathbf{B}}_t)] = \mathbb{E}[u(s, \bar{\mathbf{B}}_s)] - \mathbb{E}[g(\bar{\mathbf{B}}_t) \int_s^t \nabla \log p_w(\bar{\mathbf{B}}_w) dw] + \mathbb{E}[g(\bar{\mathbf{B}}_t) (\mathbf{k}_t - \mathbf{k}_s)].$$

Therefore, we get (15) and (14). Hence, $(\bar{\mathbf{B}}_t)_{t \in [0, T]}$ is a continuous martingale. In addition, we have that for any $t \in [0, T]$, $\mathbb{E}[\bar{\mathbf{B}}_t \bar{\mathbf{B}}_t^\top] = t \text{Id}$ and therefore, $(\bar{\mathbf{B}}_t)_{t \in [0, T]}$ is a Brownian motion using the Lévy characterisation of Brownian motion ([Revuz & Yor, 2013, Chapter IV, Theorem 3.6](#)). Denote $(\mathbf{j}_t)_{t \in [0, T]} = (\mathbf{k}_T - \mathbf{k}_{T-t})_{t \in [0, T]}$. Using (14), we have that for any $t \in [0, T]$

$$\bar{\mathbf{Y}}_t = \bar{\mathbf{Y}}_0 + \bar{\mathbf{B}}_t + \int_0^t \nabla \log p_{T-s}(\mathbf{Y}_s) ds - \mathbf{j}_t.$$

Using (13), we have for any $t \in [0, T]$

$$|\mathbf{j}|_t = \int_0^t \mathbf{1}_{\mathbf{Y}_s \in \partial\mathcal{M}} d|\mathbf{j}|_s, \quad \mathbf{j}_t = \int_0^t \mathbf{n}(\bar{\mathbf{Y}}_s) d|\mathbf{j}|_s,$$

which concludes the proof.

H. Conformational modelling of polypeptide backbones under end point constraints

Polypeptides and proteins constitute an important class of biogenic macromolecules that underpin most aspects of organic life. Accurately modelling their conformational ensembles, i.e. the set of three-dimensional structures they assume under physiological conditions, is essential to both understanding the biological function of existing and designing the enzymatic or therapeutic properties of novel proteins (Lane, 2023). Motivated by the success of diffusion models in computer vision and natural language processing, there has been considerable interest in applying them to learn and sample from distributions over the conformational space of protein structures (Watson et al., 2022; Trippe et al., 2022; Wu et al., 2022).

H.1. Problem parameterisation

Proteins are biopolymers in which a sequence of N amino acids is joined together through $N - 1$ peptide bonds, resulting in a so-called polypeptide backbone with protruding amino acid residues. As the deviation of chemical bond lengths and angles from their theoretical optimum is generally negligible, the problem of modelling the three-dimensional structure of this polypeptide chain is often reframed in the space of the internal torsion angles Φ and Ψ (see Figure 12a for an illustration), which can be modelled on a $(2N - 2)$ -dimensional torus \mathbb{T}^{2N-2} .

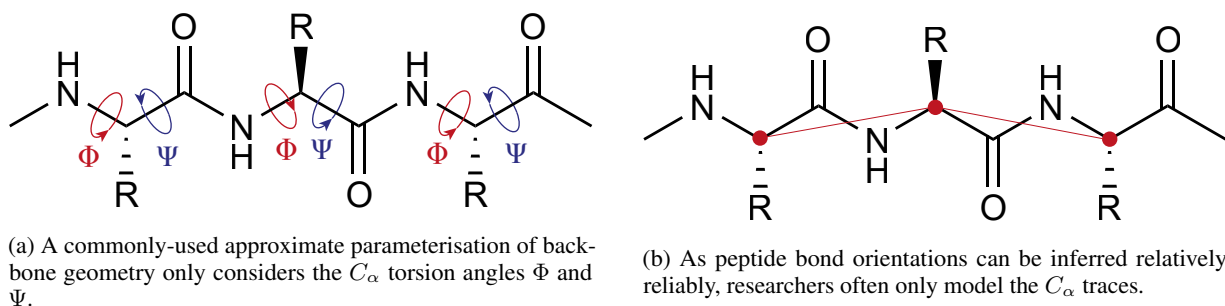


Figure 12: Widely-used approaches to modelling the conformations of polypeptide backbones.

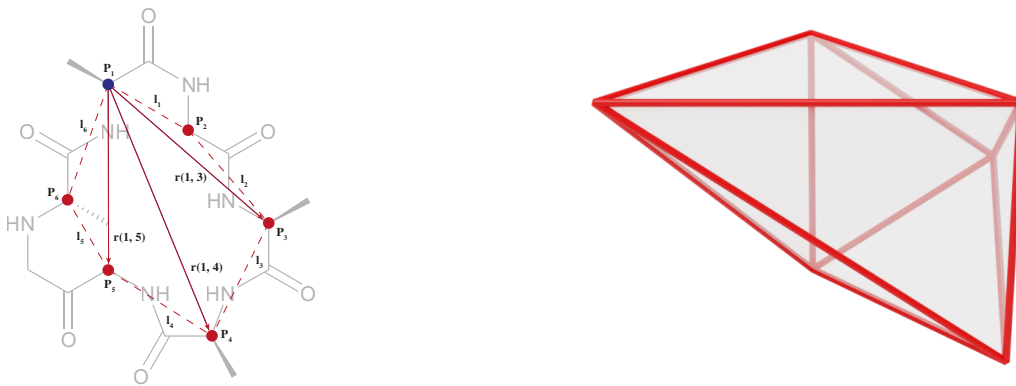
In many data-scarce practical settings such as antibody or enzyme design, it is often unnecessary or even undesirable to model the structure of an entire protein, as researchers are primarily interested in specific functional sites with distinct biochemical properties. However, generating conformational ensembles for such substructural elements necessitates positional constraints on their endpoints to ensure that they can be accommodated by the remaining scaffold. While it is conceivable that a diffusion model could derive such constraints from limited experimental data, we argue that it is much more efficient and precise to encode them explicitly.

For this purpose, we adopt the distance constraint formulation from Han & Rudolph (2006) and interpret the backbone as a spatial chain with N spherical joints and fixed-length links (see Figure 13a for an illustration). After selecting an arbitrary anchor point, the geometry of the polypeptide chain is fully specified by (a) the set of link lengths $\ell = \{\ell_j\}_{j=1}^N$, (b) the set of vectors $\mathbf{r} = \{r(1, j)\}_{j=2}^N$ between the anchor point and each atom in the chain, (c) the set of dihedral angles

$$\mathbf{T} = \left\{ \arccos \left(\frac{|\langle r(1, j) \times r(1, j+1), r(1, j+1) \times r(1, j+2) \rangle|}{|r(1, j) \times r(1, j+1)| |r(1, j+1) \times r(1, j+2)|} \right) \right\}_{j=2}^{N-2} \in \mathbb{T}^{N-3}$$

defined by any three consecutive vectors. Given an arbitrary anchor point distance $d_{\text{anchor}} = \ell_N = r(1, N)$, the set of valid vectors \mathbf{r} is given by the convex polytope $\mathbb{P} \subseteq \mathbb{R}^3$ defined by the following linear constraints:

$$\begin{aligned} r(1, 3) &\leq \ell_1 + \ell_2, \\ -r(1, 3) &\leq -|\ell_1 - \ell_2|, \\ \left. \begin{aligned} r(1, j) - r(1, j+1) &\leq \ell_j, \\ -r(1, j) + r(1, j+1) &\leq \ell_j, \\ -r(j) - r(j+1) &\leq -\ell_j, \end{aligned} \right\} 3 \leq j \leq N-2, \\ r(1, N-1) &\leq \ell_{N-1} + d_{\text{anchor}}, \\ -r(1, N-1) &\leq -|\ell_{N-1} - d_{\text{anchor}}|. \end{aligned}$$



(a) An illustrative diagram of the proposed parameterisation for modelling the C_α trace geometry of the cyclic peptide C-AAGAGG.

(b) The convex polytope constraining the diagonals of the triangles for the given bond lengths in the illustrated molecule. The total design space is the product of this polytope with the 4D flat torus.

Figure 13: Parameterising the conformational space of polypeptide backbones under anchor point distance constraints.

This means that the set of all valid polypeptide backbone conformations is defined by the product manifold $\mathbb{P} \times \mathbb{T}^{N-3}$, enabling us to train diffusion models that exclusively generate conformations with a fixed anchor point distance d_{anchor} .

H.2. Data generation and model training

As a proof-of-concept for the practicality of our methods, we chose to model the conformational distribution of the cyclic peptide C-AAGAGG (see Figure 13). Cyclic peptides are an increasingly important drug modality with therapeutic uses ranging from antimicrobials to oncology, exhibiting circular polypeptide backbones that confer a range of desirable pharmacodynamic and pharmacokinetic properties (Dougherty et al., 2019). To reduce the dimensionality of the problem, we only consider the C_α traces (with fixed C_α - C'_α link distances of 3.6 \AA) instead of the full polypeptide backbone (see Figure 12b), although we note that our framework is fully applicable to both settings.

To derive a suitable dataset, the product manifold describing the conformations of cyclic C_α traces of length $N = 6$, i.e. $\mathbb{P} \times \mathbb{T}^3$, was constructed and used to generate 10^7 uniform samples satisfying the anchor point distance constraint $d_{\text{anchor}} = 0$. Subsequently, an estimate of the free energy E_i of each sample i was obtained by (1) reconstructing the full-atom peptide from each C_α trace using the PULCHRA algorithm (Rotkiewicz & Skolnick, 2008), (2) relaxing all non- C_α backbone and side-chain atoms (keeping the C_α positions fixed), and (3) modelling the potential energy of each of the resulting conformations using the OPENMM suite of molecular dynamics tools (Eastman et al., 2017), and the AMBER force field (Hornak et al., 2006). These free energy estimates were then used to approximate the Boltzmann distribution over conformational states

$$p_B(i) \propto \exp\left(-\frac{E_i}{k_B T}\right),$$

where temperature was set to $T = 273.15K$ and $k_B = 1.380649 \cdot 10^{-23} J \cdot K^{-1}$ is the Boltzmann constant. As the potential energy surfaces of polypeptides are known to be relatively rough (Krivov & Karplus, 2004), the resulting distribution was moderately smoothed by running forward Brownian motion on both the polytope and the torus for 100 steps, using a small step size of 10^{-2} and the respective metrics. Finally, a sample of 10^6 C_α traces was drawn from this distribution and used for training and evaluating our models.

I. Configurational modelling of robotic arms under manipulability constraints

Accurately determining and specifying the movement of a robotic arm and the forces it exerts is a fundamental problem in many real-world robotics applications. A widely-used set of descriptors for modelling the flexibility of a given joint configuration are so-called manipulability ellipsoids (Yoshikawa, 1985), which are kinetostatic performance measures that quantify the ability to move or exert forces along different directions. Jaquier et al. (2021) present a geometric framework to learn trajectories of manipulability ellipsoids by making use of the fact any ellipsoid $M \in \mathbb{R}^N$ is defined by the set of points $\{\mathbf{x} | \mathbf{x}^T \mathbf{A} \mathbf{x} = 1\}$ where \mathbf{A} lies on the manifold of $N \times N$ symmetric positive definite matrices S_{++}^N .

In many practical settings, it is desirable to constrain the minimal or maximal volume of a manipulability ellipsoid to retain motional flexibility or limit the magnitude of the exerted force. This necessitates lower or upper limits on the determinant of \mathbf{A} , translating into constraints on S_{++}^N . To model this, we make use of one of the datasets introduced by Jaquier et al. (2021), containing demonstrations of a robotic arm drawing different letters in the plane, providing the respective positional trajectories (\mathbb{R}^2) and velocity manipulability ellipsoids (S_{++}^2).

We use the processing routines provided by Jaquier et al. (2021) to interpolate the trajectories into 10^4 distinct points, for each of which we derive the position $\mathbf{x} \in \mathbb{R}^2$ and the PSD matrix

$$\mathbf{A} = \begin{pmatrix} a & b \\ b & c \end{pmatrix} \in S_{++}^2.$$

parametrizing the velocity manipulability ellipsoid $M \in \mathbb{R}^2$. The resulting data is split into training, validation, and test sets by trajectory and visualized in Figures 14 and 15.

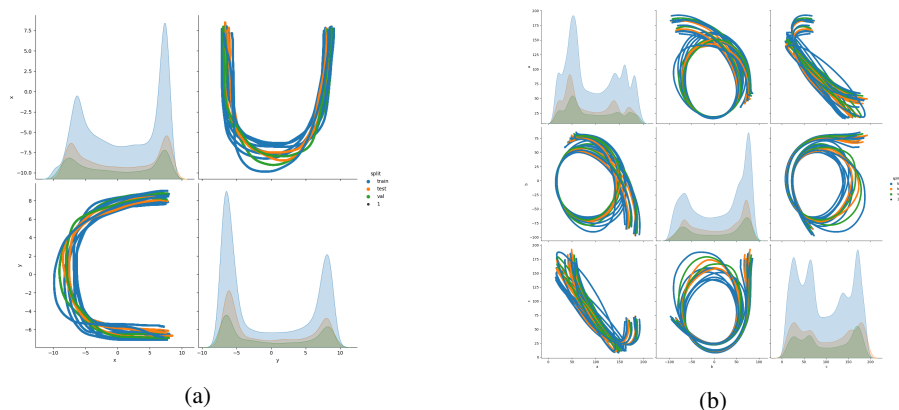


Figure 14: Positional trajectories $\mathbf{x} \in \mathbb{R}^2$ (a) and the parameters a, b, c of the the SPD matrix $\mathbf{A} \in S_{++}^2$ (b) for the letter C.

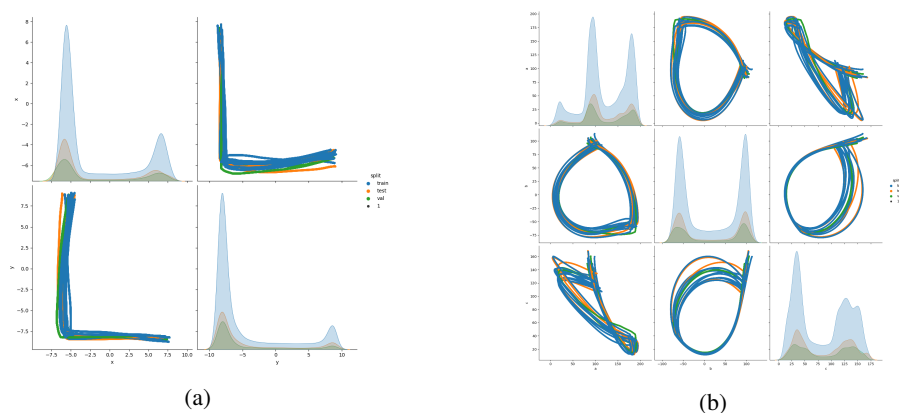


Figure 15: Positional trajectories $\mathbf{x} \in \mathbb{R}^2$ (a) and the parameters a, b, c of the the SPD matrix $\mathbf{A} \in S_{++}^2$ (b) for the letter L.

J. Experimental details

In what follows we describe the experimental settings used to generate results introduced in Section 5. The models and experiments have been implemented in Jax (Bradbury et al., 2018), using a modified version of the Riemannian geometry library Geomstats (Miolane et al., 2020).

Architecture. The architecture of the score network s_θ is given by a multilayer perceptron with 6 hidden layers with 512 units each. We use sinusoidal activation functions.

Training. All models are trained by the stochastic optimizer Adam (Kingma & Ba, 2014) with parameters $\beta_1 = 0.9$, $\beta_2 = 0.999$, batch-size of 256 data-points. The learning rate is annealed with a linear ramp from 0 to 1000 steps, reaching the maximum value of $2e - 4$, and from then with a cosine schedule down to 0 after $100k$ iterations in total.

Diffusion. Following Song et al. (2021), the diffusion models diffusion coefficient is parametrized as $g(t) = \sqrt{\beta(t)}$ with $\beta : t \mapsto \beta_{\min} + (\beta_{\max} - \beta_{\min}) \cdot t$, where we found $\beta_{\min} = 0.001$ and $\beta_{\max} = 6$ to work best.

Metrics. We measure the performance of trained models via the Maximum Mean Discrepancy (MMD) (Gretton et al., 2012), which is a kernel based metric between two distributions P and Q . The MMD can be empirically approximated with the following U-statistics $\text{MMD}^2(P, Q) = \frac{1}{m(m-1)} \sum_i \sum_{j \neq i} k(x_i, x_j) + \frac{1}{m(m-1)} \sum_i \sum_{j \neq i} k(y_i, y_j) - 2 \frac{1}{m^2} \sum_i \sum_j k(x_i, y_j)$ with $x_i \sim P$ and $y_i \sim Q$, where k is a kernel.

Low temperature sampling. As in Ingraham et al. (2022), we use low temperature sampling in order to trade-off fidelity for diversity. It combines to ingredients: 1. an approximation of the corrector sampling Song et al. (2021), 2. a low temperature approximation of the target p . Namely, instead of targeting p_0 we target $p_0^{\lambda_0}$ (unnormalised density). We refer to Ingraham et al. (2022, Appendix B) for details about the derivation. Recall that we consider the following SDE in the backward process

$$d\overleftarrow{\mathbf{X}}_t = \beta_{T-t} \left\{ \frac{1}{2} \overleftarrow{\mathbf{X}}_t + s_\theta(T-t, \overleftarrow{\mathbf{X}}_t) \right\} dt + \beta_t^{1/2} d\mathbf{B}_t.$$

The updated scheme is given by

$$d\overleftarrow{\mathbf{X}}_t = \beta_{T-t} \left\{ \frac{1}{2} \overleftarrow{\mathbf{X}}_t + (\lambda_t + \frac{\lambda_0 \Psi}{2}) s_\theta(T-t, \overleftarrow{\mathbf{X}}_t) \right\} dt + (1 + \Psi)^{1/2} \beta_t^{1/2} d\mathbf{B}_t,$$

where $\lambda_t = \lambda_0 / (\alpha_t + (1 - \alpha_t) \lambda_0)$ and $\alpha_t = \exp[-2 \int_0^t \beta_s ds]$. In practice λ_0 controls the concentration of the measure while Ψ controls the strength of the corrector. We use $\Psi = 0$ as we do not consider a corrector term and perform a sweep over the parameters $\lambda_0 \in \{1, 2, 3, 5, 10\}$.

J.1. Synthetic data on polytopes

Hypercube $[-1, 1]^n$. The hypercube is a specific instance of a convex polytope where the affine constraints are given by the following coefficients:

$$A = \begin{pmatrix} 1 & \dots & 0 \\ -1 & \dots & 0 \\ \vdots & \ddots & \vdots \\ 0 & \dots & 1 \\ 0 & \dots & -1 \end{pmatrix}, \quad b = \begin{pmatrix} 1 \\ 1 \\ \vdots \\ 1 \\ 1 \end{pmatrix}.$$

Where A is a $2n \times n$ matrix and b an n dimensional vector.

We construct the training and test datasets by sampling for both 100000 points from a mixture of ‘wrapped normal’ distributions illustrated in Figure 16a and which density is given by

$$p_0(x) = 0.7 \text{ReflectedStep}[(0.5, 0.5), \cdot, \{f_i\}_{i \in \mathcal{I}}] \# \mathcal{N}(0, 0.25) + 0.3 \text{ReflectedStep}[(-0.5, -0.5), \cdot, \{f_i\}_{i \in \mathcal{I}}] \# \mathcal{N}(0, 0.25).$$

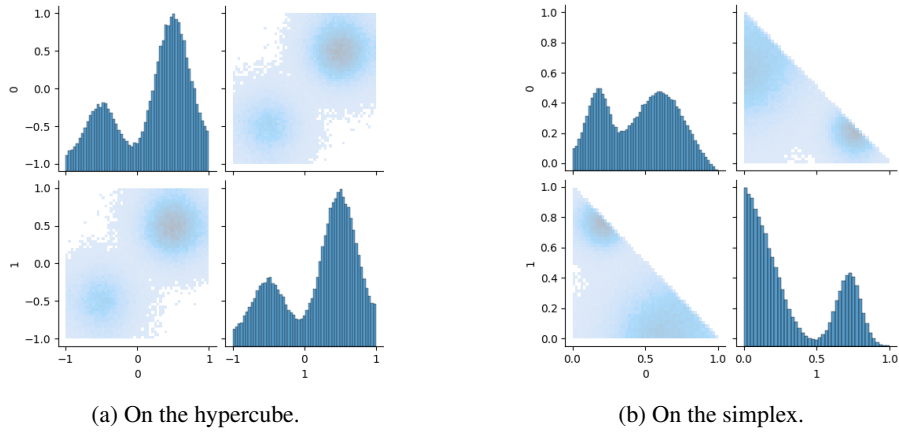


Figure 16: Pairwise and marginals samples from the synthetic data distribution.

Simplex Δ^n . Similarly, to parameterise the simplex as a convex polytope we set the matrix and constraints to be given by

$$A = \begin{pmatrix} -1 & 0 & \dots & 0 \\ \vdots & \vdots & \ddots & \vdots \\ 0 & 0 & \dots & -1 \\ 1 & 1 & 1 & 1 \end{pmatrix}, \quad b = \begin{pmatrix} 0 \\ \vdots \\ 0 \\ 1 \end{pmatrix}.$$

Where A will be a $n - 1 \times n$ matrix. Essentially we perform diffusion over the first $n - 1$ components of the simplex, allowing the last component to be determined by the one minus the sum of the first $n - 1$.

Similarly than for the hypercube, we construct the training and test datasets from generated data points which are illustrated in Figure 16b. The score network at different times is illustrated in Figure 17.

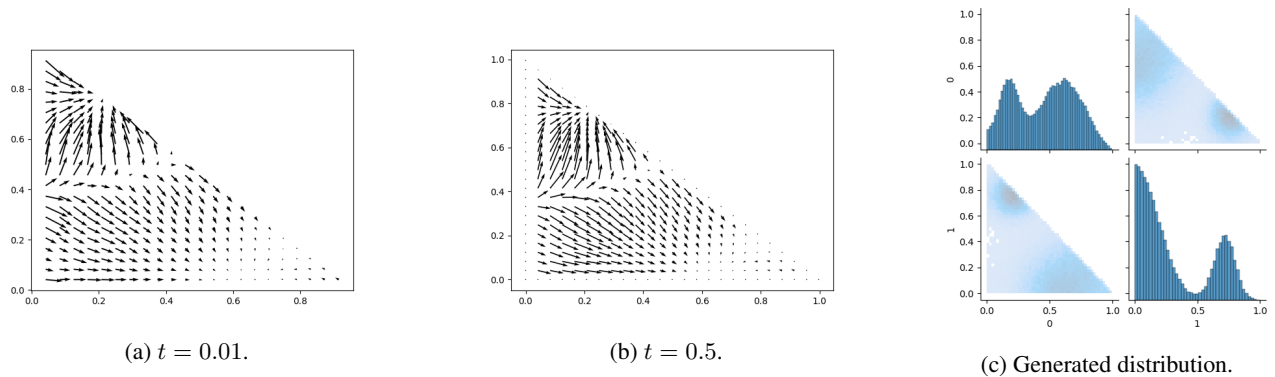


Figure 17: Evolution of the score on the simplex and generated distribution.

The Birkhoff polytope. The Birkhoff polytope is the space of doubly stochastic matrices, i.e. $B_n = \{P \in [0, 1]^{n \times n} : \sum_i P_{i,j} = 1, \sum_j P_{i,j} = 1\}$. It is a convex polytope in \mathbb{R}^{n^2} and has dimension $d = (n - 1)^2$.

Diffusion Models for Constrained Domains

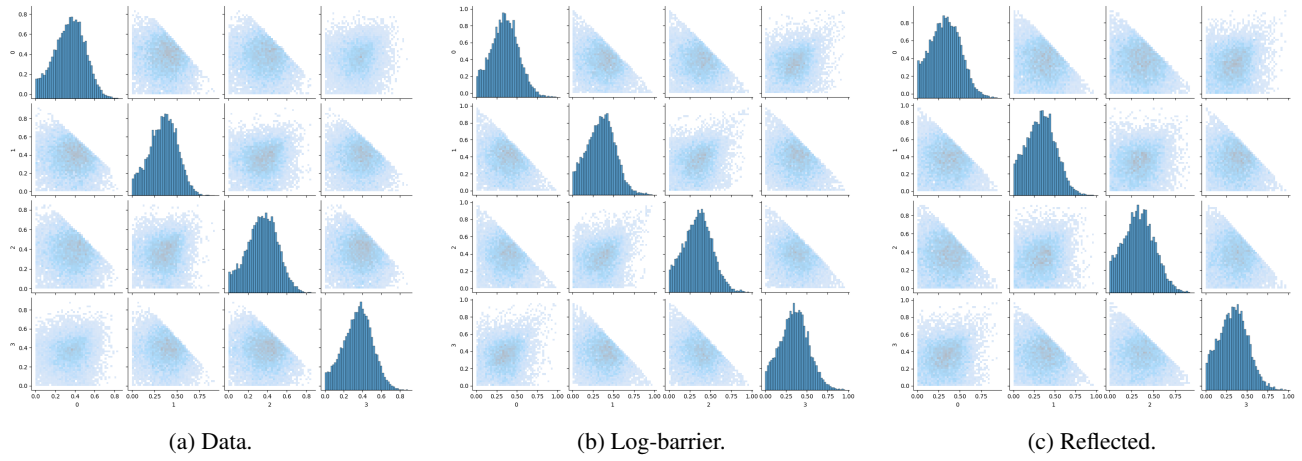


Figure 18: Pairwise and marginals samples on the Birkhoff polytope from synthetic data distribution and from trained constrained diffusion models.